Tau-centric multi-target approach for Alzheimer's disease: development of first-in-class dual glycogen synthase kinase 3β and tau-aggregation inhibitors

Annachiara Gandini,[a,b] Manuela Bartolini,[a] Daniele Tedesco,[a] Loreto Martinez-Gonzalez,[c] Carlos Roca,[c] Nuria E. Campillo,[c] Josefa Zaldivar-Diez,[c] Concepción Perez,[d] Giampaolo Zuccheri,[a,e] Andrea Miti,[a,e] Alessandra Feoli,[f] Sabrina Castellano,[f] Sabrina Petralla,[a] Barbara Monti,[a] Martina Rossi,[b] Fabio Moda,[g] Giuseppe Legname,[b] Ana Martinez,[c] Maria Laura Bolognesi*,[a]

(a) Department of Pharmacy and Biotechnology, Alma Mater Studiorum - University of Bologna, Via Belmeloro 6, I-40126 Bologna, Italy; (b) Laboratory of Prion Biology, Department of Neuroscience, Scuola Internazionale Superiore di Studi Avanzati (SISSA), Via Bonomea 265, I-34136 Trieste, Italy; (c) Centro de Investigaciones Biologica, CSIC, Ramiro de Maeztu 9, 28040 Madrid, Spain; (d) Instituto de Quimica Medica, CSIC, Calle Juan de la Cierva 3, 28006 Madrid, Spain; (e) S3 Center of the Institute of Nanosciences, Italian National Research Council (CNR); (f) EpigeneticMedChemLab, Department of Pharmacy, University of Salerno, Via Giovanni Paolo II 132, I-84084 Fisciano, Italy; (g) IRCCS Foundation Carlo Besta Neurological Institute, via Celoria 11, I-20133 Milan, Italy.

Abstract

Several findings propose altered tau protein network as an important target for Alzheimer's disease (AD). Particularly, two points of pharmacological intervention can be envisaged: inhibition of phosphorylating tau kinase GSK-3β, and tau aggregation process. In light of this and based on our interest in multi-target paradigms in AD, we report on the discovery of 2,4-thiazolidinedione-derivatives endowed with such profile. **28** and **30** displayed micromolar IC_{50} values towards GSK-3β, together with the capacity of inhibiting AcPHF6 aggregation of 60% and 80% at 10 μM, respectively. In addition, they showed PAMPA-BBB permeability, together with a suitable cellular safety profile. **30** also displayed inhibition of both K18 and full-length tau aggregations. Finally, both compounds were able to improve cell viability in an okadaic acid-induced neurodegeneration cell model. To the best of our knowledge, **28** and **30** are the first balanced, non-toxic, dual-acting compounds hitting tau cascade at two different hubs.

1. Introduction

Drug development for Alzheimer's disease (AD) has proven to be very difficult. A 0.4% success rate for approval is among the lowest for any therapeutic area and it has been 15 years since the last drug, memantine, was launched.[1] What is even more discouraging is that despite the enormous social and economic rewards of a successful treatment, big pharma are pulling out of AD research.[2,3]

Over the years, some of the complications of AD drug discovery have been related to its multi-factorial nature. Advances in systems biology have been revealing a phenotypic robustness and a network structure for AD pathology strongly implying that single-target compounds are inadequate in curing AD and preventing its progression.[4-6] Conversely, a polypharmacological approach appears better suited to confront such a complex disease and to provide disease-modifying effects.[7,8] In light of this, the development of multi-target directed ligands (MTDLs), i.e. small molecules able to hit multiple targets responsible for AD pathogenesis, has been pursued as a promising therapeutic opportunity in recent years, leading to the discovery of different promising compounds.[9-12] In spite of the clear pre-clinical success, no rationally designed multi-target compound has been approved so far for the treatment of AD.[13] Indeed, AD multi-target drug discovery combines the hurdles of an extremely challenging area, with those of novel pharmaceutical tools.

Clearly, to develop clinically-effective MTDLs, the selection of appropriate targets is of utmost importance. They should be causally linked to the most relevant AD pathological processes and their 'networking' is critical for determining the final properties of the MTDL.[13]

The amyloid hypothesis[14] has long been the central dogma in AD drug discovery, leading to many (either single or multi-target)[15-17] drug candidates. However, recently this hypothesis has been questioned on the basis of the repeating failures of β-amyloid (Aβ)-based drugs.[18-22] In parallel, several findings are suggesting that the altered tau network is more significant than the Aβ one from a pathogenic point of view.[23] Strikingly, the very close spatial correlation between neuronal loss

and tau aggregates in patients' brains, and the genetic evidence for the role of tau aggregation in a wide range of neurodegenerative disorders due to mutations in the tau gene, provides a strong foundation to tau-targeted therapy.[24]

Tau is a microtubule-associated protein (MAP), predominantly expressed in the neuronal axons where it promotes microtubule stabilization and facilitates axonal transport of proteins, trophic factors, and other cellular constituents, including neurotransmitters.[25, 26] Under physiological conditions, tau is in a dynamic equilibrium between the microtubule-bound and -unbound states, regulated by specific kinases and phosphatases. However, under pathological conditions, hyperphosphorylated tau loses its microtubules stabilizing and axonal transport functions. Particularly, hyperphosphorylated tau becomes prone to misfolding and aggregation, ultimately resulting in the formation of neurofibrillary tangles (NFTs) (Figure 1). The tau aggregation cascade, once initiated, is self-replicating, depleting the physiological tau pool in the neuron, and converting it to toxic NFTs, which continue to accumulate, leading to neuronal death.[25, 26] In view of all these evidences, tau cascade is being recognized as a promising target for the development of drug candidates for the treatment of AD.[27-29]

Building on these considerations, we aimed to identify novel MTDLs able to hit tau cascade at two validated hubs, namely by inhibiting glycogen synthase kinase 3β (GSK-3β) and tau aggregation process (Figure 1).

GSK-3β is a multifunctional serine/threonine kinase that phosphorylate tau mainly at the Ser199, Ser396, and Ser413 sites.[30] In AD, GSK-3β over-expression induces tau hyperphosphorylation, and consequently, its disjunction from the microtubules and its aggregation. Moreover, GSK-3β has an important role in other AD key features such as inflammation and apoptosis.[31]

Over the past decade, an increased interest in GSK-3β led to the discovery of several inhibitors, with different chemical scaffolds and mechanisms of action (i.e. ATP competition, allosteric modulation, and irreversible inhibition). [30, 31] There was considerable rationale from preclinical models that GSK-3β inhibitors could be disease-modifying drugs. [30, 31] Importantly, the ATP non-

competitive GSK-3β inhibitor tideglusib (**1** in Figure 2), is currently under clinical development for AD and other tauopathies and has demonstrated no safety concerns even after long-term treatments.[31]
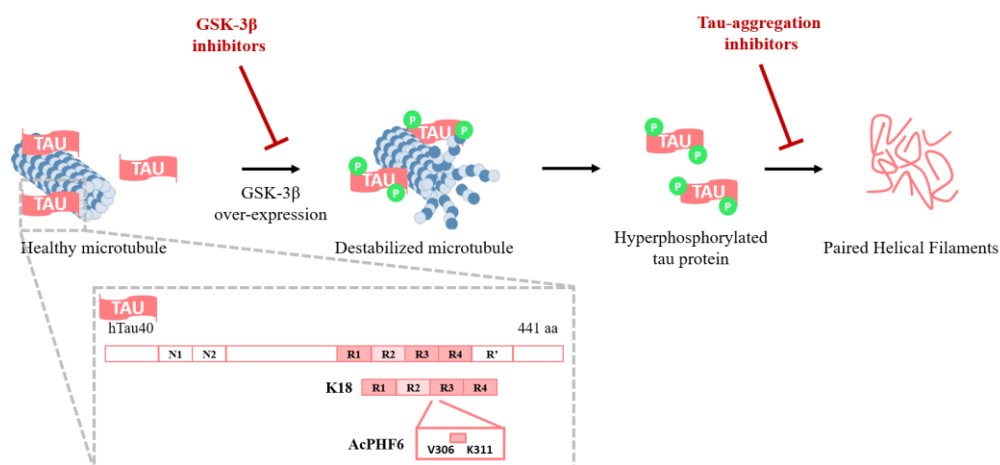
Figure 1. Schematic depiction of tau cascade, tau structure, and points of pharmacological intervention.

On the other side, agents capable of preventing tau self-assembly represent another attractive strategy for the treatment of AD.[32] Importantly, phenothiazine derivatives methylene blue (**2** in Figure 2) and LMTX (**3** in Figure 2) are in clinical phase of AD drug development.[33, 34]
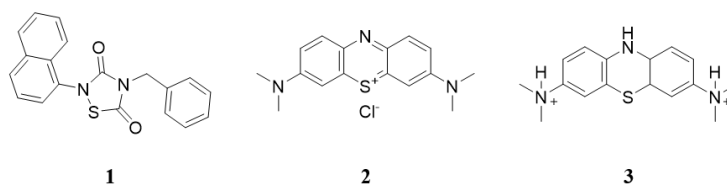
Figure 2. Chemical structures of tau-directed AD investigational drugs **1**-**3**.

Herein, we report on the development of the first-in-class MTDLs **4**-**38** (general structure in Figure 3) which, by simultaneously inhibiting GSK-3β and the tau aggregation process, may pave the way for a completely novel AD treatment. In contrast with the available single-targeted drug candidates,

their superior potential efficacy is based on the assumption that, by targeting two points of the tau network, they could trigger a synergistic response, and eliminate compensatory reactions and feedback controls, thereby overcoming the pathway robustness. Furthermore, in principle, such dual inhibitors should possess a lower target-related toxicity. Because most links in neuronal networks are weak, it can be inferred that even low-affinity dual inhibitors should be sufficient to achieve a significant anti-tau effect. If the concentration required to obtain the desired effect is lower with respect to single-targeted drugs, the risk for toxicity is reduced.[35] This greatly eases the constraints of druggability, which is a key issue for GSK-3β.[31]

To note, although interesting examples of MTDLs that combine anti-tau activity with a second one beneficial for AD treatment have been recently reported (e.g. anti-amyloid, anti-oxidant, anti-inflammatory activity),[36-46] **4**-**38** are the first compounds able to hit tau cascade at two hubs.

2. Design of dual GSK-3β/tau aggregation inhibitors

Designing a ligand able to simultaneously bind two targets sharing no similarity in the binding sites, as it is the case of GSK-3β and tau protein, could be very challenging.[47] Likewise, combining the molecular frameworks of two CNS-directed single-target ligands (or the corresponding underlying pharmacophores) in one small molecule might not be an easy task, especially in terms of pharmacokinetics optimization.[13]
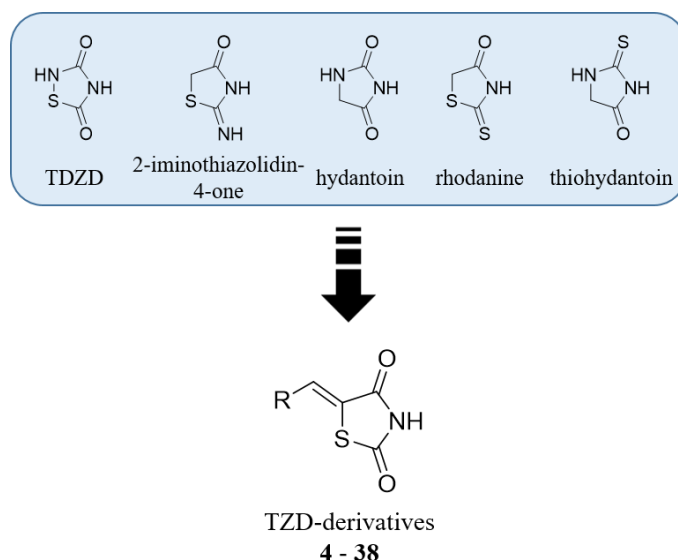
Figure 3. General chemical structures of TDZD, 2-iminothiazolidin-4-one, hydantoin, rhodanine, thiohydantoin, and TZD-derivatives **4**-**38**.

In this context, 5-membered heterocyclic fragments caught our attention. Several known GSK-3β inhibitors carry 5-membered heterocyclic rings (i.e. 2-iminothiazolidin-4-one and hydantoin, Figure 3) with hydrogen bond acceptor and donor functionalities.[48, 49] Thiadiazolidinediones (TDZDs, exemplified by **1**) have been reported as the first class of non-ATP competitive inhibitors of GSK-3β.[50] Intriguingly, rhodanine, thiohydantoin and hydantoin isosters (Figure 3) were discovered by Mandelkow and Waldmann as effective tau anti-aggregation motifs.[51] These derivatives inhibited the formation of tau aggregates in a dose-dependent fashion, as well as destabilized preformed tau aggregates. The ability of rhodanines and thiohydantoins to directly interact with tau aggregates has been confirmed by the tau imaging properties of derivatives RH1 ((Z)-ethyl 2-(5-((5-(3-iodophenyl)furan-2-yl)methylene)-4-oxo-2-thioxothiazolidin-3-yl) acetate) and TH2 ((Z)-ethyl 2-(4-((5-(3-iodophenyl)furan-2-yl)methylene)-5-oxo-2-thioxoimidazolidin-1-yl) acetate).[52] Thus, we reasoned that the cross-talk between all these fragments could be favorably exploited to identify MTDLs directed to the two selected targets (i.e. GSK-3β and tau protein).

In principle, being prone to bind a large number of targets with weak or moderate affinity, rhodanines might be an optimal starting point for ligand-based multi-target endeavors.[53]

Nevertheless, the validity of rhodanine scaffold is questionable because of its notorious Pan Assay Interference Compounds (PAINS) behavior.[53] Although it is hard to draw the line between true multi-target activity and aggregation effects or potential reactivity, which may or may not[54-56] lead to assay interference, we considered safer to disregard the rhodanine scaffold.

Conversely, among the 5-membered heterocycle isosters, we selected the 2,4-thiazolidinedione (TZD, Figure 3) scaffold, which has never been explored as either GSK-3β or tau anti-aggregation fragment. As highlighted by Baell and Pouliot,[57-59] the TZD core itself does not aggressively drive assay interference in the same way as rhodanine does. Indeed, TZD is not identified as a PAIN by computational filters (see "PAINS analysis" in Experimental Section). To support the drug-likeness of the TZD scaffold in AD, the TZD-based antidiabetic drug pioglitazone (PIO) is currently under evaluation in a Phase 3 clinical trial as an anti-inflammatory drug in mild cognitive impaired patients.[60]

Starting from the TZD, as a first step, we decided to decorate it at position 5 with different aromatic and heteroaromatic substituents, affording a 35-membered library of 5-arylidene-2,4-thiazolidinediones (**4-38**, Table 1). This was based on previous studies showing that (i) 5-arylidene substitution improved affinity in a series of 2-iminothiazolidin-4-one competitive GSK-3β inhibitors; (ii) due to their volume and size, they do not fit in similar regions of homologous kinases, therefore showing selectivity for GSK-3β.[49] In addition, this would allow to maintain the planarity and aromaticity features, critical for interaction with tau fibrils.[61] Among the possible aromatic and heteroaromatic substituents, we included those (e.g. indoles, benzofurans and benzothiophenes) reported as effective anti-amyloid scaffolds.[62]

3. Chemistry

The synthesis of **4-38** was easily achieved through a one-pot, optimized version of the Knoevenagel condensation. The conventional protocol based on the reaction of equimolar amounts of TZD and an aromatic aldehyde,[63] in the presence of catalytic amounts of pyridine and acetic acid, suffers

from several disadvantages, such as long reaction times, low to moderate yields, use of toxic solvents. To overcome these drawbacks, a solvent-free procedure using ethylenediamine diacetate (EDDA) as an inexpensive and effective Brönsted acid-base catalyst has been proposed.[64] Clearly, there are several advantages in using a solvent-free reaction, such as reduced pollution, lower costs, simplicity in process and handling, shorter reaction times, and higher yields. With the aim of further improving the green chemistry aspects, we performed the reaction under microwave (MW) irradiation. Thus, a newly optimized procedure based on the solvent-free condensation of aromatic aldehydes with TZD (1:1) in the presence of EDDA (0.5 eq), under MW irradiation at 80°C, for 30 minutes (Scheme 1) was developed. It was successfully applied to the vast array of aldehydes **4a-38a** (with electron-withdrawing and electron-donating groups, heteroaromatic, conjugated and planar rings) to obtain target compounds **4-38** (see Table 1 for structures). To the best of our knowledge, microwave-mediated EDDA-catalyzed Knoevenagel condensation has never been exploited so far for the synthesis of 5-arylidene-2,4-thiazolidinediones.

Scheme 1. Optimized Knoevenagel reaction for the synthesis of TZD-derivatives **4-38**.

4a - 38a TZD **4 - 38** (18-92%)
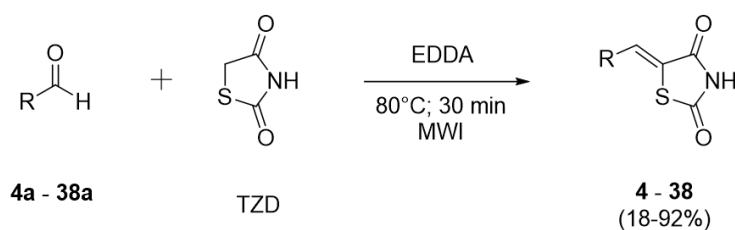
All the aromatic aldehydes were purchased from commercial vendors, except **14a** and **15a**. These were synthesized by slightly modified reported procedures (Scheme 2).[65, 66] In the first case, 2-fluorobenzaldehyde (**39**) was reacted with dimethylamine in the presence of potassium carbonate to provide aldehyde **14a**. In the second case, the commercially available 3-(dimethylamino)benzyl alcohol (**40**) was oxidized under Swern conditions, affording aldehyde **15a**.

Scheme 2. Synthetic procedure for the synthesis of aldehydes **14a** and **15a**.
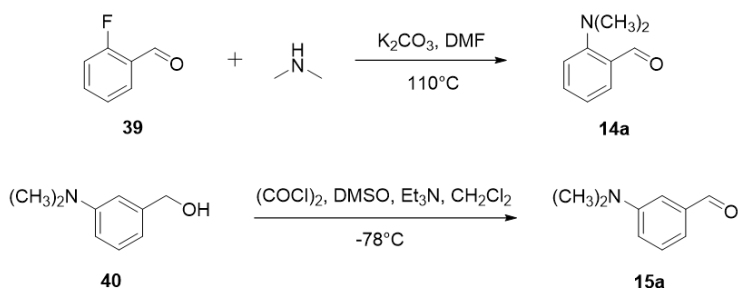
All compounds were characterized using analytical (HPLC) and spectroscopic data (^{1}H- and ^{13}C-NMR, ESI-MS), which are collected in the Experimental Section and Supporting Information.
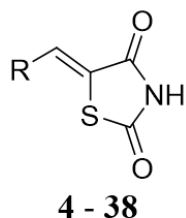
4. Results and discussion

To verify the capability of the synthesized molecules to simultaneously hit the two targets and to make a judicious use of resources, we designed a screening pipeline, whose main goals were: (i) to make a preliminary screening of all synthesized molecules for GSK-3β activity; (ii) to assess blood-brain barrier (BBB) permeability of the active GSK-3β inhibitors; (iii) to filter out toxic compounds; (iv) to assess the most promising compounds for their anti-tau activity; (iv) to confirm the anti-tau activity in a cellular model.

GSK-3β inhibition assays
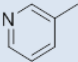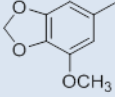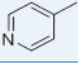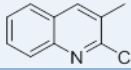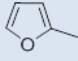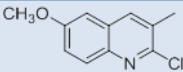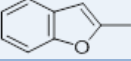
GSK-3β biochemical inhibition for **4-38** was first assessed using the Kinase-Glo luminescent assay, which quantifies the decrease in ATP levels following the kinase reaction.[67] All compounds were first tested at 10 μM, and hits with percentage inhibition ≥50% were further tested to obtain IC$_{50}$ values (determined by using the linear regression parameter). TDZD8 (4-benzyl-2-methyl-1,2,4-thiadiazolidine-3,5-dione)[50] was used as reference compound. Encouragingly, sixteen out of the starting thirty-five TZDs inhibited GSK-3β with IC$_{50}$ values in the single-digit micromolar range

(Table 1). Compound **30** ((Z)-5-((5-methoxy-1-methyl-1H-indol-3-yl)methylene)thiazolidine-2,4-dione) was the most active, with a submicromolar IC_{50} of 0.89 ± 0.21 µM.

Table 1. GSK-3β inhibition evaluation of TZD-derivatives **4-38**.

4 - 38

cmpd no.	R	GSK-3β IC_{50} (µM)	cmpd no.	R	GSK-3β IC_{50} (µM)
4	phenyl	>10	22	2-thienyl	7.99 ± 0.57
5	2-hydroxyphenyl	>10	23	benzothiophen-2-yl	7.47 ± 0.85
6	3-hydroxyphenyl	>10	24	2-naphthyl	>10
7	4-hydroxyphenyl	8.99 ± 0.78	25	9-anthracenyl	>10
8	3-methoxy-4-hydroxyphenyl	7.08 ± 0.51	26	styryl	>10
9	2-methoxy-4-hydroxyphenyl	6.01 ± 0.72	27	4-(dimethylamino)styryl	>10
10	2-hydroxy-3-nitrophenyl	9.22 ± 0.90	28	3-methyl-1H-indol-3-yl	4.93 ± 0.66
11	2-fluorophenyl	>10	29	5-methoxy-3-methyl-1H-indol-3-yl	>10
12	3-fluorophenyl	>10	30	5-methoxy-1-methyl-1H-indol-3-yl	0.89 ± 0.21
13	4-fluorophenyl	>10	31	1,2-dimethylbenzimidazol-2-yl	>10
14	2-(N(CH₃)₂)phenyl	9.22 ± 0.89	32	2-phenyl-1H-indol-3-yl	6.03 ± 0.44
15	3-((CH₃)₂N)phenyl	8.54 ± 0.81	33	4-biphenyl	>10
16	4-((CH₃)₂N)phenyl	>10	34	2-(benzyloxy)phenyl	>10
17	2-pyridyl	>10	35	2,3-dihydro-1,4-benzodioxin-6-yl	7.01 ± 0.61

18		8.75 ± 0.77	36		>10
19		1.42 ± 0.12	37		6.13 ± 0.43
20		>10	38		3.55 ± 0.23
21		>10	TDZD8		0.69 ± 0.09

From the data reported in Table 1, preliminary structure-activity relationships (SAR) can be drawn. In comparison with unsubstituted **4** ($IC_{50} > 10$ μM), hydroxyl substituents in *ortho* and *meta* positions of the phenyl ring did not increase enzyme inhibition, as evident for **5** and **6**. On the other side, -OH substitution in *para* improved the inhibitory activity, as shown by **7** (8.99 ± 0.78 μM). Di-substituted **8**-**10** did not show any significant enhancement with respect to **7**. Addition of the fluorine atom seemed not to affect the activity. Regarding the dimethylamino substituents, the favored positions are the *ortho* and *meta*, as shown by **14** (9.22 ± 0.89 μM) and **15** (8.54 ± 0.81 μM). Replacement of the phenyl of **4** with a 4-pyridil ring, as in **19**, led to an IC_{50} of 1.42 ± 0.12 μM. Thiophene and benzothiophene substitutions (**22**, **23**) also resulted in a good inhibitory activity. In contrast, substitution with bulky moieties such as naphthyl, anthracene, phenylpropylen or biphenyl, as in **24**-**27**, **33**, and **34**, resulted in compounds inactive at 10 μM. Interestingly, bicyclic N-heterocycles, such as **28**-**32**, showed different behaviors. More hydrophilic **28** and **32** are better GSK-3β inhibitors than **29**. Moreover, the insertion of a methyl group on the nitrogen atom of the indole, as in **30**, resulted in an important improvement in the inhibitory profile (0.89 ± 0.21 μM). This trend in activity had already been described for previously reported indolyl-maleimide series of GSK-3β inhibitors.[68] A retrospective computational study was performed to rationalize these results and predict compound binding mode (see Supporting Information).

The GSK-3β inhibitory activity of selected inhibitors **28** and **30** (vide infra) was also confirmed in a Time-Resolved Fluorescence Energy Transfer (TR-FRET) assay. **28** and **30** were tested at ten different concentrations and the resulting dose-response curves are depicted in Figure 4. The obtained IC_{50} values for both **28** (21 ± 2.4 μM) and **30** (5.5 ± 0.8 μM) were in agreement with the

ones obtained with the Kinase-Glo Luminescent Kinase Assay. Thus, we were able to prove the genuine GSK-3β inhibitory activity of **28** and **30**. In addition, because of the presence of the alkylidene moiety, prone to potential covalent reactions (see "PAINS analysis" for further discussion), we aimed to assess the reversibility of GSK-3β inhibition. Thus, we performed a jump-dilution experiment on **30**,[94] demonstrating that the enzymatic activity was restored after dilution, pointing to a reversible inhibition by **30** (see Figure S6).
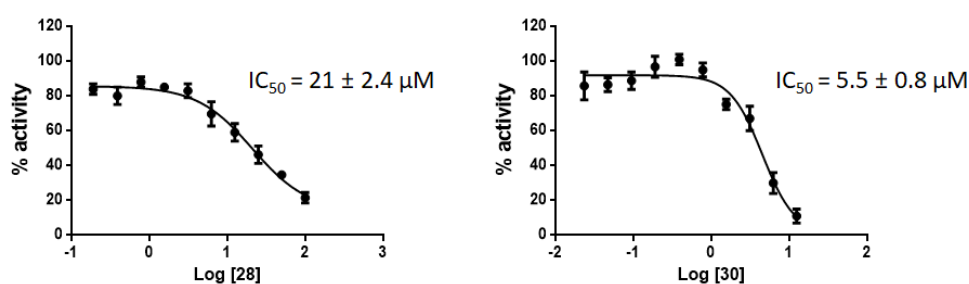
Figure 4. Dose-response curves of GSK-3β activity in the presence of **28** and **30**. Values are the means ± SD determined for at least two separate experiments.

To further investigate the mechanism of action, **28** and **30** were subjected to kinetic analysis. Particularly, we determined the competition with the ATP. We varied both ATP and **28** and **30** concentrations with a constant concentration of GS-2, the substrate used in the enzymatic reaction. The double-reciprocal plot of data (Figure 5) indicates that both **28** and **30** act as competitive inhibitors of ATP binding. In light of this, TZD derivatives represent a new chemical class of ATP-competitive GSK-3β inhibitors.
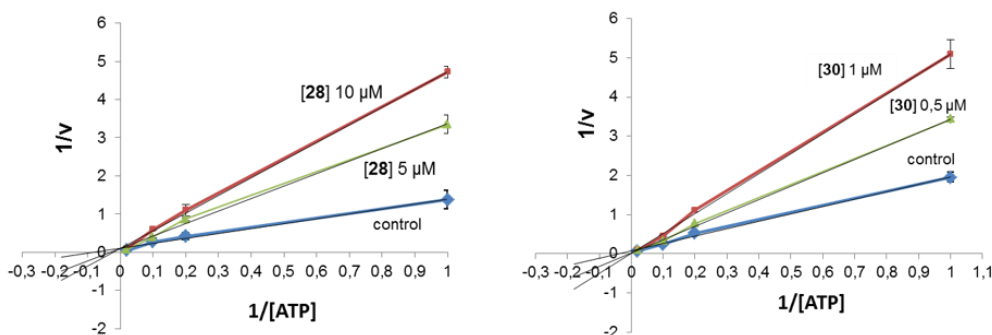
Figure 5. Kinetic data for the TZD-derivatives **28** and **30**. ATP concentration in the reaction mixture varied from 1 to 50 µM. Compounds concentrations used are depicted in the plot, and the concentration of GS-2 was kept constant at 25 µM. Each point is the mean of two different experiments, both analyzed in triplicate.

Blood Brain Barrier permeation

One of the main obstacles for CNS drug discovery is the drug penetration into the BBB at therapeutic concentrations.[69] Parallel Artificial Membrane Permeability Assay (PAMPA)-BBB is a high throughput technique developed to predict BBB passive permeability. In order to preliminary explore the capacity of GSK-3β inhibitors **7**, **8-10, 14, 15, 18, 19**, **22**, **23**, **28**, **30**, **32**, **35**, **37**, **38** to penetrate into the brain, we used the PAMPA-BBB method,[70] which employs a brain lipid porcine membrane. The in vitro effective permeability (P_e) of commercial drugs through lipid membrane extract together with TZD-derivatives was determined. An assay validation was made comparing the reported permeability values of commercial drugs with the experimental data. A good correlation between experimental-described values was obtained (Figure S5). From this equation and following the pattern established in the literature for BBB permeation prediction,[71] we could classify compounds as CNS+ when they present a permeability > 3.07 x 10^{-6} cm/s. Based on these results, only compounds **14**, **15**, **23**, **28**, and **30** are predicted to cross the BBB by passive permeation (Table S2), and thus were progressed for toxicity and tau anti-aggregation analysis.

Neuro- and hepato-toxicity assessment

The failure of several AD drug discovery approaches has been widely attributed not only to the lack of efficacy, but also to the toxicity of the drug candidates after a chronic treatment.[1] In consideration of this, and motivated by the promising in vitro results, we first tested neurotoxicity on the five GSK-3β inhibitors predicted to cross the BBB, in comparison to PIO (Figure 6).

Primary cultures of cerebellar granule neurons (CGNs) are an useful *in vitro* models to study neuronal death.[72] MTT (3-(4,5-dimethylthiazol-2-yl)-2,5-diphenyltetrazolium bromide) assessment of CGNs viability after 24 h treatment with **14**, **15**, and **23** showed a clear toxic effect for all the three compounds, as well as PIO, even at 5 μM concentration. Notably, **28** and **30** showed a very low neurotoxicity only at the highest tested concentrations (50 μM).

In AD patients, aging, comorbidity, and subsequent polytherapy significantly contribute to increase the risk of drug-drug interactions and, consequently, hepatotoxicity. Moreover, although being effective therapeutic agents, some TZD derivatives have been reported to show hepatotoxicity.[73] To this end, parallel experiments were performed on **14**, **15**, **23**, **28**, and **30** in a human hepatoma cell line (HepG2) in comparison with PIO (Figure 6). After 24 h incubation at 0-50 μM, a concentration-dependent decrease in cell viability was observed for PIO, **14**, and **15**. Encouragingly, compounds **23**, **28**, and **30** showed no hepatotoxicity, even at 50 μM. On the basis of the toxicity profiles, indole derivatives **28** and **30** emerged as the most drug-like compounds.
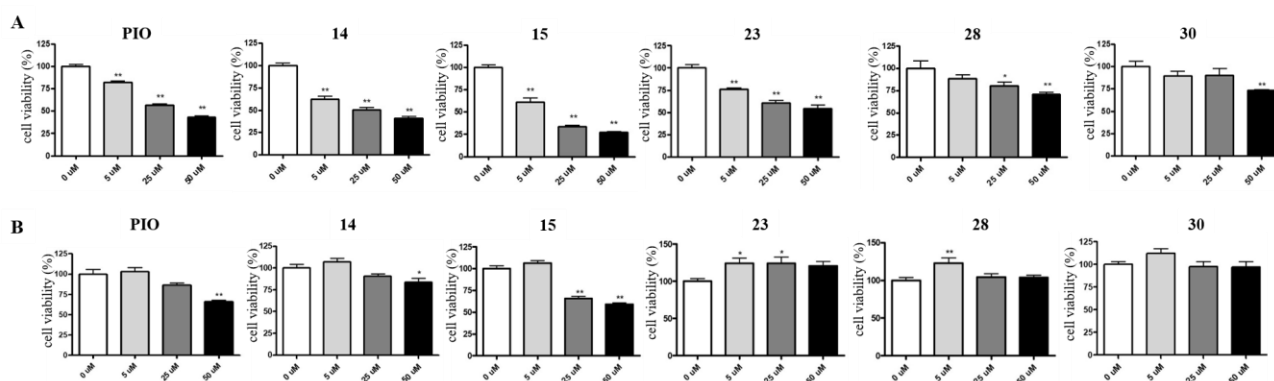

Figure 6. (A) Neurotoxicity on primary rat cerebellar granule neurons (CGNs) after 24 h treatment. (B) Hepatotoxicity on human hepatoma cells (HepG2) after 24 h treatment. Results are expressed as

percentage of controls and are the mean ± SE of at least 3 different experiments, each run in triplicate.

AcPHF6 aggregation and inhibition studies by Thioflavin T (ThT) fluorescence, circular dichroism spectroscopy and atomic force microscopy

In parallel, the ability of BBB-permeable GSK-3β inhibitors **14**, **15**, **23**, **28**, and **30** to interfere with tau aggregation in vitro was investigated using the AcPHF6 peptide ($_{306}$VQIVYK$_{311}$) as a model system. Indeed, AcPHF6 is a short segment found in the third repeat of the microtubule-binding region of tau protein (Figure 1). As recently highlighted by cryo-electron microscopy of tau filaments, $_{306}$VQIVYK$_{311}$ spatially arranges into a beta-strand conformation and contributes to the formation of the C-shaped cross-β structure representing the filament core of PHFs.[74] As AcPHF6 undergoes to spontaneous fibrillation, it has been proposed as a suitable model for screening small molecule inhibitors of tau aggregation.[75-80] As for other β-sheet proteins, the aggregation process can be monitored by fluorescence in the presence of ThT, which displays a characteristic change in the emission spectrum in the presence of β-rich structures.[81] The anti-aggregating activity of **14**, **15**, **23**, **28**, and **30** was therefore monitored in phosphate buffer 50 mM pH 7.4 using ThT as detection dye. In agreement with previous studies,[75-80] when incubated alone, AcPHF6 rapidly aggregated, as confirmed by the increase in the fluorescence intensity over a period of 80 min (Figure 7). Co-incubation of AcPHF6 with the selected compounds led to a significant (>50%) decrease of the fluorescence intensities, indicating that all compounds could significantly interfere with AcPHF6 aggregation, even if at different extents (from 54.7% to 79.8%). In particular, derivatives **15** and **30** showed the highest inhibitory potencies reducing the fluorescence signal at plateau by almost 80% (79.5 and 79.8%, respectively) and resulting only slightly less potent than the known inhibitor myricetin.[82] Figure 7B shows the details of the kinetics of aggregation of AcPHF6 incubated alone and in the presence of compounds **28** and **30**, namely the derivatives endowed with the best safety profile (see above).
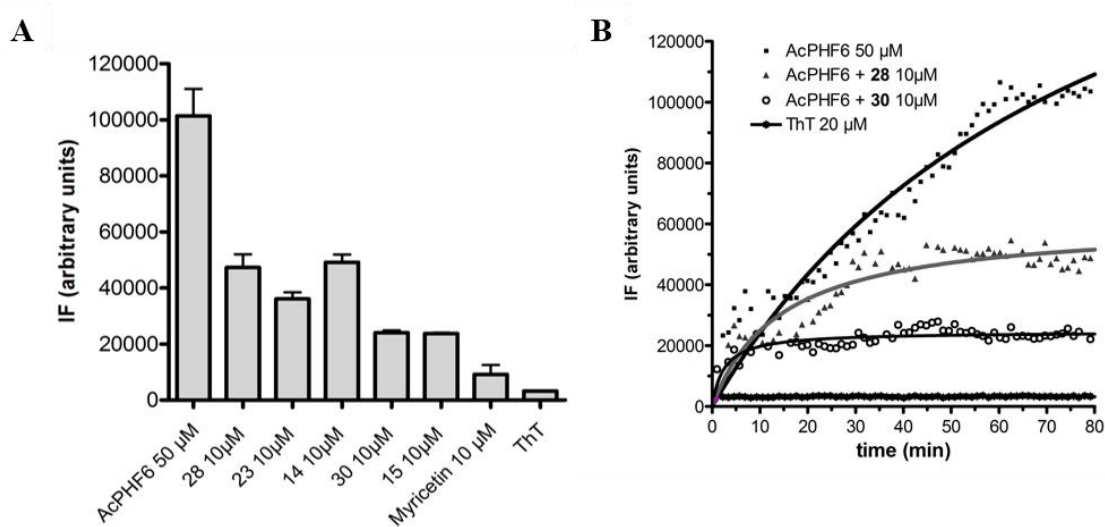
Figure 7. (A) Inhibition of AcPHF6 peptide (50 µM) aggregation in the presence of selected derivatives (10 µM) after 80 min incubation. The data are the mean of at least three repeats. (B) Kinetics of the AcPHF6 aggregation in the absence and in the presence of compounds **28** and **30** monitored by ThT fluorescence.

Circular dichroism (CD) studies were then carried out to gain further insights into the mechanism of inhibition of **28** and **30** and to exclude false positive outcomes due to the possible displacement of bound ThT by the tested compounds. The CD spectrum of AcPHF6 (Figure 8) shows a negative band at 221 nm followed by a positive band at shorter wavelengths, both of which are typical features of β-sheet structures. A decrease in intensity was observed for the CD spectrum of AcPHF6 in the presence of **28**, suggesting that the abundance of β-sheet structures is lower. On the other hand, the CD profile of AcPHF6 in the presence of **30** lacks for the typical bands of β-sheet structures, with the peptide displaying an unordered conformation. Both behaviors are consistent with the inhibitory trends highlighted by the fluorescence-based assay; therefore, CD data confirm the inhibitory capacity of derivatives **28** and **30** and suggest that their anti-aggregating activity is related to their ability to stabilize the AcPHF6 peptide in a less fibrillogenic conformation, with derivative **30** being much more effective in doing so.
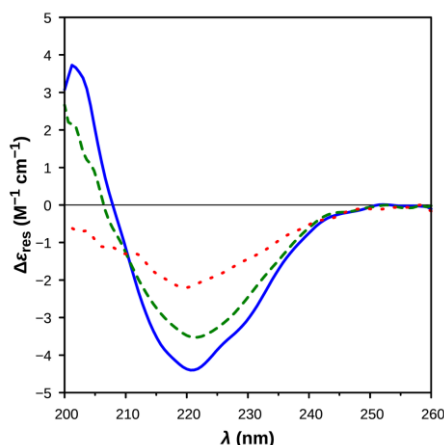
Figure 8. CD spectra of AcPHF6 (100 µM) in the absence (*solid*) and in the presence of **28** (20 µM, *dashed*) or **30** (20 µM, *dotted*), measured after 2 h incubation. Solvent: phosphate buffer (50 mM pH 7.4)/water/methanol/DMSO 89:10:0.95:0.05 (v/v/v/v). Pathlength: 1 mm.

Atomic force microscopy (AFM) studies were also performed to examine the morphology of the fibrils formed by a 50 µM phosphate buffer solution AcPHF6 peptide alone and in the presence of **28** and **30**, when prepared in the same conditions employed for the above-described ThT studies (but in the absence of ThT) and CD studies. After solution incubation, aliquots of the solutions were subjected to ultrafiltration to separate the low molecular weight un-polymerized hexapeptide fraction from the high-molecular weight fiber fraction, and such high-molecular weight fraction was adsorbed on the surface of mica for AFM imaging. We believe that the presence of un-polymerized peptides at the time of AFM specimen preparation could be at least partly responsible for some confusing results sometimes attributed to AFM imaging of amyloids.[22] As evident in the micrographs in Figure 9, long and thick amyloid fibrils were imaged after adsorbing on mica the solution of AcPHF6 incubated in the absence of inhibitor compounds (Figure 9A). Here, fibers with individual diameters of 10 nm or more (and lengths of several hundreds of nanometers) are found in bundles and higher-order aggregates. On the other hand, only much smaller structures (possibly oligomers or protofibrils) were observed from the adsorption of the hexapeptide incubated in the

presence of the inhibitors **28** and **30** (Figure 9B and C). We can hypothesize that such lower molecular weight aggregated structures (peptide oligomers or protofibrils) could be responsible for the small but non-zero ThT fluorescence signal recorded during the incubation of the hexapeptide in the presence of **28** and **30**..
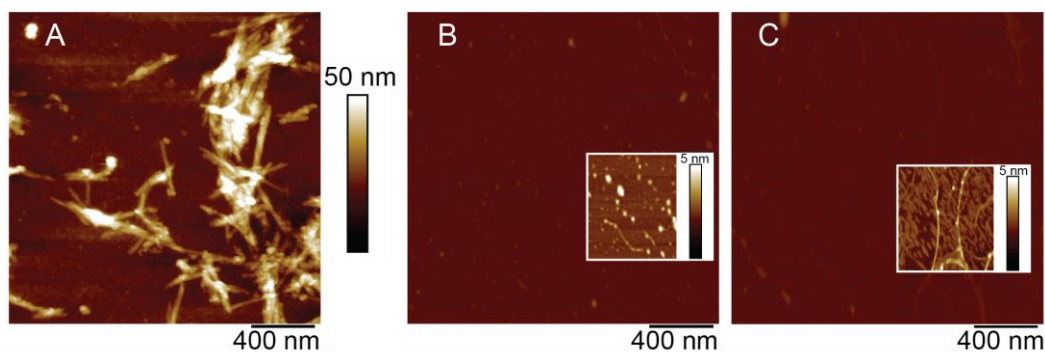
Figure 9. AFM micrographs of amyloid fibers obtained from the aggregation of 50 µM AcPHF6 peptide in phosphate buffer in the absence (A), and in the presence of 10 µM compound **28** (B) and compound **30** (C). The height of fibers on the mica substrate is coded according to the common included color table (ranging from 0 to 50 nm of heights) as to allow visual comparison of the different size of the adsorbed structures. Insets of panels B and C: the rectangular portions of panels B and C situated at the inset location in the micrograph (and of the size of the inset) are displayed according to the reported magnified 0-5 nm color look-up table in order to better show the smaller and thinner adsorbed structures.

K18 and full-length tau aggregation and inhibition studies

Encouraged by the results obtained with the AcPHF6 peptide, we decided to confirm the anti-aggregating properties of the most active **30** in more clinically relevant models of tau aggregation. The tau fibrillization process can be replicated in vitro, however, recombinant tau shows very little intrinsic tendency to aggregate due to the lack of a series of post-translational modifications required for its aggregation. Indeed, during the last years, recombinant truncated tau isoforms are more frequently used for in vitro tau aggregation, where the addition of anionic co-factors (e.g.

heparin, arachidonic acid) results in the formation of fibrils that resemble those observed in the brains of AD patients.[83, 84] Thus, **30** was firstly evaluated in a heparin-induced tau assembly assay, in which the fibrillization of the truncated K18 tau fragment (comprising four microtubules-binding repeats, Figure 1) was monitored by ThT. The aggregation of the tau fragment K18 was achieved through the Real-Time Quaking-Induced Conversion (RT-QuIC) technique.[85] As shown in Figure 10, K18 alone was completely aggregated after 11-12 h and the fluorescence intensity reached the highest value, while the treatment with **30** (1, 5, 10 µM) resulted in a delay of K18 self-aggregation. Moreover, the analysis of the averaged fluorescence intensities at the plateau of the kinetic showed a 35% inhibition of the aggregation process.
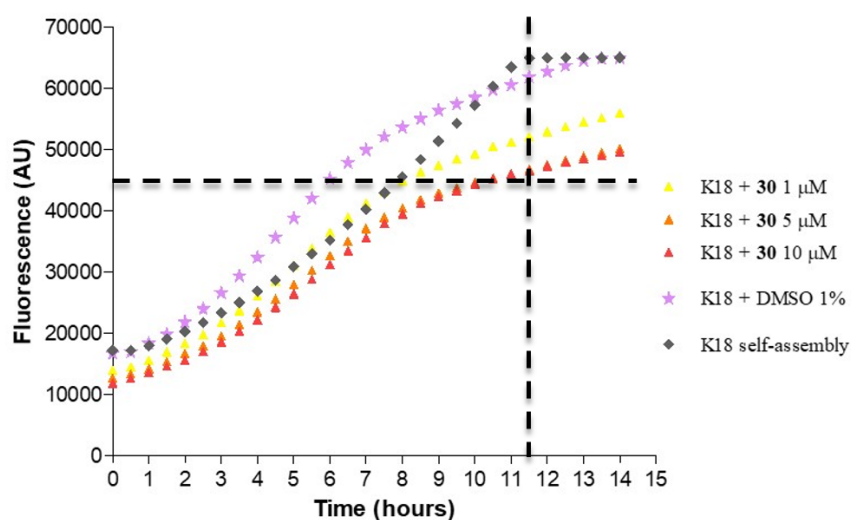
Figure 10. RT-QuIC analysis of **30** activity on tau K18 self-aggregation monitored by ThT fluorescence.

Motivated by the promising results, we also tested the inhibitory activity of **30** towards the heparin-induced self-aggregation of full-length 2N4R tau, through RT-QuIC technique. Treatment of 2N4R tau with **30** (10 µM) did not show a delay in the aggregation process, as can be seen from Figure 11. However, from the analysis of the averaged fluorescence intensities at the plateau of the kinetic, **30**

shows a 30% inhibition of the aggregation process. Importantly, this result is in agreement with that obtained with K18 fragment, confirming the potential of **30** as tau anti-aggregating compound.
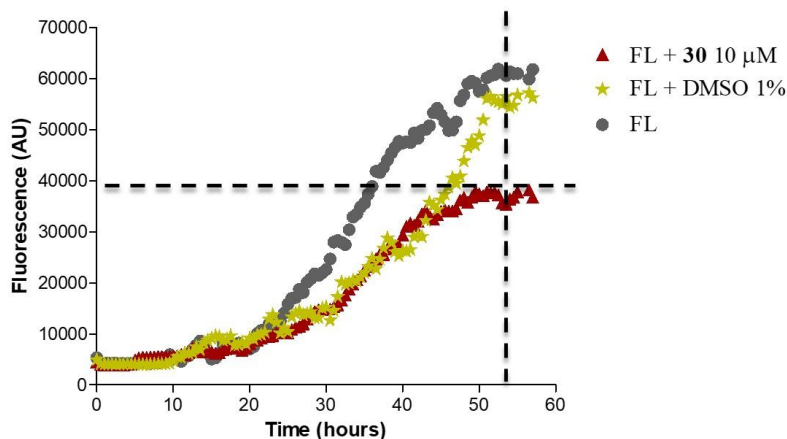
Figure 11. RT-QuIC analysis of **30** activity on full-length tau self-aggregation monitored by ThT fluorescence.

Okadaic acid-induced tau hyperphosphorylation cell model

Increasing evidence has suggested that inhibition of phosphatases by okadaic acid (OA) represents the most robust way to induce tau hyperphosphorylation. Thus, OA-treated cell lines and primary neuronal cultures have been used as established cellular models of hyperphosphorylated tau-induced neurodegeneration.[86, 87] In addition, OA-treated rodents recapitulate the morphological hallmarks of AD.[88]

To confirm the anti-tau profile of **28** and **30** in a cellular context, we further explored their rescue potential in the OA-induced neurodegeneration cell model, in comparison with TDZD8.[50]

We studied the effect of **28** and **30** and TDZD8, at two different concentrations (10 and 20 μM), in a human neuroblastoma cell line (SH-SY5Y) treated with OA (Figure 12). As expected, OA induced a decrease in cell viability higher than 50%. Importantly, both **28** and **30** were able to increase the cell viability probably due to the decrease on tau phosphorylation by GSK-3β

inhibition. Particularly, **28** was only slightly less effective than TDZD8. To note, other indole derivatives have been reported as effective in counteracting OA-induced neurotoxicity.[43]
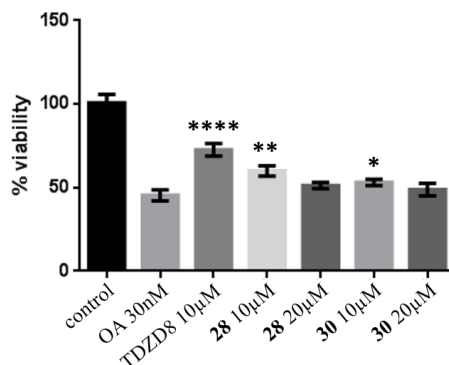
Figure 12. OA-induced neurodegeneration cell model. Effects of treatment with **28** and **30**. Results are mean value ± SEM, represented as relatives to control value (=100), of n=6 from three independent experiments.

Inhibitory activity profile towards casein kinase 1 (CK1) δ and ε, and cell division cycle 7 (Cdc7)

Finally, to preliminarily address kinase promiscuity issues of ATP competitive inhibitors,[89] we tested **28** and **30** on three selected kinases, i.e. casein kinase 1 (CK1) δ and ε, and cell division cycle 7 (Cdc7) kinase, available in our laboratories. Cdc7 is another representative cell cycle regulation kinase,[90] which should show low binding affinity toward new GSK-3β hits to avoid possible toxicities. CK1δ and CK1ε represent GSK-3β phylogenetically diverse kinases, able to phosphorylate tau.[91]

Therefore, the inhibition of **28** and **30** toward CK1δ, CK1ε, Cdc7 and GSK-3β were assessed at 10 μM. Encouragingly, **28** and **30** only poorly, or not inhibited at all, CK1δ, CK1ε, and Cdc7 (Figure 13), while they inhibited GSK-3β by 95% and 100%, respectively. This reveals a preliminary selectivity of both **28** and **30** towards GSK-3β.
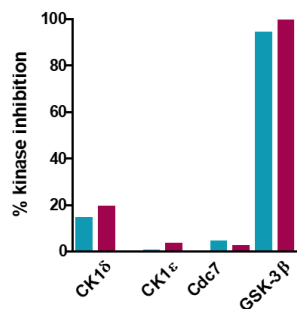
Figure 13. Inhibitory activity profile of **28** (blue) and **30** (purple) towards human CK1δ, CK1ε, Cdc7 and GSK-3β kinases, at a fixed concentration of 10 μM.

5. Conclusions

We have been interested in MTDLs that can confront the multifactorial nature of AD for years. Recently, in accordance with the drug discovery trends, we argued that a single molecule able to act at two tau validated targets belonging to the tau cascade might have clinical benefit and show higher therapeutic potential than those addressing the amyloid cascade.

Although in principle very promising, this approach must deal with the problem of targeting two proteins with no binding site similarity.

On the basis of structural resemblances, as well as the available SAR data for GSK-3β and amyloid aggregation inhibitors, we were able to select the thiazolidinedione as a starting scaffold and to design a novel, first-in-class chemical series of dual inhibitors.

A library of thirty-five derivatives was synthesized and tested in a pipeline tailored to our academic setting. This has delivered two hit molecules (**28** and **30**) that display features we consider relevant in terms of MTDL drug discovery principles: (i) they are low molecular weight fragment hits with evident advantages in terms of intended "promiscuity" and pharmacokinetic properties; (ii) their activity is balanced; (iii) they show no significant toxicity, even towards mammalian primary neuronal cells.

Thus, although very preliminary, the collected results show that it is possible to design small molecules that act specifically at two structurally different tau targets, like a kinase and a fibrillar

protein, with a good potency and in the same concentration range to yield compounds effective at a cellular level.

These hits, targeting two independent but interrelated activities, might serve as tools to validate a completely new tau-centric network approach as a potential new disease-modifying strategy to treat AD.

6. Experimental section

Chemistry

All the commercial available reagents and solvents were purchased from Sigma-Aldrich, Alpha Aesar, VWR, and TCI, and used without further purification. Reactions were followed by analytical thin layer chromatography (TLC), on pre-coated TLC plates (layer 0.20 mm silica gel60 with a fluorescent indicator UV254, from Sigma-Aldrich). Developed plates were air-dried and analyzed under a UV lamp (UV 254/365 nm). CEM Discover SP focused microwave reactor was used for microwave mediated reactions. Nuclear magnetic resonance (NMR) experiments were run on Varian VXR 400 (400 MHz for ^{1}H, 100 MHz for ^{13}C). ^{1}H and ^{13}C NMR spectra were acquired at 300 K using deuterated dimethyl sulfoxide $((CD_3)_2SO)$ and chloroform $(CDCl_3)$ as solvents. Chemical shifts (δ) are reported in parts per million (ppm) relative to tetramethylsilane (TMS) as internal reference, and coupling constants (J) are reported in hertz (Hz). The spin multiplicities are reported as s (singlet), br s (broad singlet), d (doublet), t (triplet), q (quartet), and m (multiplet). Mass spectra were recorded on a VG707EH-F apparatus, and electrospray ionization (ESI) both in positive and negative mode was applied. Compounds were named following IUPAC rules as applied by ChemBioDraw Ultra (version 14.0). All of the final compounds showed ≥95% purity by analytical HPLC (see Table S3). As reported in literature,[92] the TZD-derivatives **4**-**38** were obtained as single Z isomers. Indeed, their ^{1}H-NMR spectra shows only one signal attributable to the resonance of the 5-methylidene proton in the range 7.50-8.70 ppm; while in their ^{13}C-NMR spectra

the 5-methylidene carbon and the C5 of the TZD ring resonated in the ranges 130.5-140.7 and 117.5-128.0 ppm, respectively.

PAINS analysis

Aware of the liabilities that might arise from the alkylidene-TZD scaffold, we have analyzed **4-38** for known classes of assay interference compounds.[93] First, **4-38** were not recognized as PAINS according to the Free ADME-Tox Filtering Tool (FAF-Drugs4) program (http://fafdrugs4.mti.univ-paris-diderot.fr/), and to the "False Positive Remover" software (http://www.cbligand.org/PAINS/), neither as aggregators according to the software "Aggregator Advisor" (http://advisor.bkslab.org/). However, FAF-Drugs4 labeled them as covalent inhibitors due to their electrophilic nature. Thus, we provided evidences that the activities reported herein are highly likely not caused by pan assay interference.

First, the genuine GSK-3β inhibitory activity of **28** and **30** has been confirmed in two assays (i.e. Kinase-Glo and TR-FRET). Possible promiscuous kinase inhibition was preliminary ruled out by the fact that **28** and **30** do not inhibit similar kinases (CK1δ, CK1ε) and Cdc7.

As regards tau aggregation inhibition, activities of **28** and **30** has been evaluated in three different assays (i.e. ThT-based fluorimetric assay, CD, and AFM), which show consistent results.

Concerning the potential unspecific covalent reactions with proteins of alkylidene-TZD, we first investigated the thiol-trapping reactivity of **28** and **30** in a simple NMR-based assay.[95] Reaction of Michael acceptor-bearing compounds with two equivalents of 2-aminoethanethiol (cysteamine), a biologically relevant model thiol,[96] in DMSO should lead to the instantaneous formation of the corresponding Michael adduct and the simultaneous disappearance of the olefin signals. In contrast to what is reported for 5-benzylidene barbiturates,[97] reaction of **28** and **30** (0.01 mmol) with cysteamine (0.02 mmol), after 30 minutes, did not lead to the formation of the Michael adduct (Figure 14). The same was observed after 24 h. Thus, we can expect that the double bond of **28** and **30** did not react covalently with sulphur nucleophiles, with indiscriminate reactivity. In addition,

based on the results of the jump-dilution and the ATP-competition assays, we are confident that they did not react covalently with GSK-3β kinase.
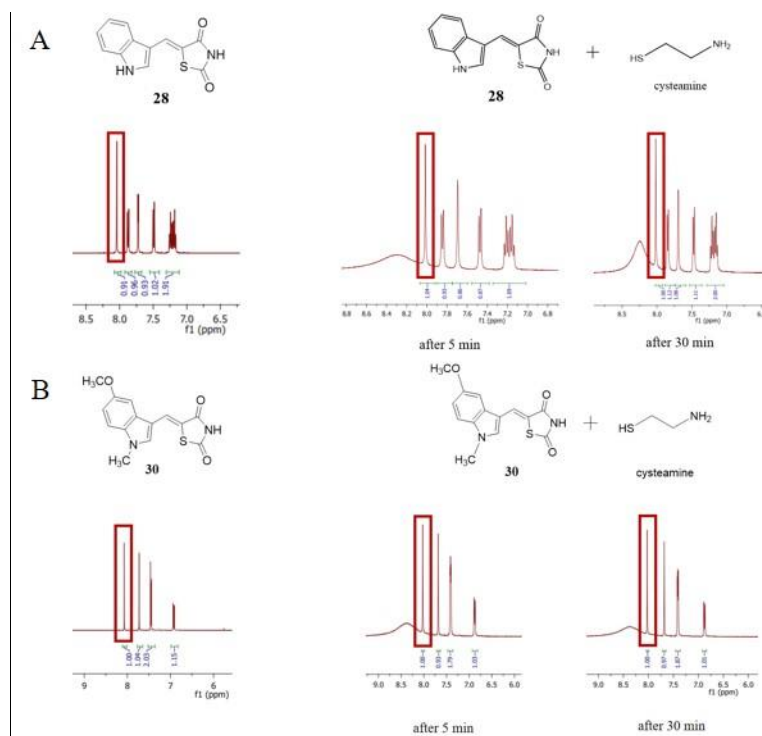
Figure 14. Thiol trapping assay. ^{1}H-NMR spectrum of **28** (A) and **30** (B) in DMSO-d_6 and in DMSO-d_6 with cysteamine (1:2). In the squares, the olefin signal is highlighted No reaction occurs, even after 30 minutes.

General procedure for the synthesis of compounds 4-38.

The corresponding aldehydes (1 mmol) were reacted with 2,4-thiazolidinedione (1 mmol), using EDDA (0.5 mmol) under microwave irradiation at 80°C for 30 minutes. The reaction mixture was diluted with water and the solid was collected by filtration. After washing it with water all the final compounds were purified through crystallization from ethanol/water.

(Z)-5-benzylidenethiazolidine-2,4-dione (4). The title compound **4** was obtained as a light yellow solid, according to general procedure using benzaldehyde (**4a**). Yield 87%. ^{1}H-NMR (401 MHz, d_6-DMSO): δ 12.61 (br s, 1H); δ 7.79 (s, 1H); δ 7.61-7.46 (m, 5H). ^{13}C-NMR (101 MHz, d_6-DMSO): δ 168.37; δ 167.89; δ 133.49; δ 132.10; δ 130.81; δ 130.41; δ 129.74; δ 124.11. MS (ESI$^-$) m/z: 204 [M-H]$^-$.

(Z)-5-(2-hydroxybenzylidene)thiazolidine-2,4-dione (5). The title compound **5** was obtained as a yellow solid, according to general procedure using 2-hydroxybenzaldehyde (**5a**). Yield 56%. ^{1}H-NMR (401 MHz, d$_6$-DMSO): δ 12.48 (br s, exch, 1H); δ 10.48 (s, exch, 1H); δ 8.02 (s, 1H); δ 7.33-7.28 (m, 2H); δ 6.96-6.92 (m, 2H). ^{13}C-NMR (101 MHz, d$_6$-DMSO): δ 168.60; δ 167.97; δ 157.69; δ 132.66; δ 128.73; δ 127.41; δ 122.36; δ 120.37; δ 120.11; δ 116.55. MS (ESI$^-$) m/z: 220 [M-H]$^-$.

(Z)-5-(3-hydroxybenzylidene)thiazolidine-2,4-dione (6). The title compound **6** was obtained as a white solid, according to general procedure using 3-hydroxybenzaldehyde (**6a**). Yield 43%. ^{1}H-NMR (401 MHz, d$_6$-DMSO): δ 12.58 (br s, exch, 1H); δ 9.82 (s, exch, 1H); δ 7.68 (s, 1H); δ 7.32 (t, *J* = 7.9, 1H); δ 7.03 (d, *J* = 7.6, 1H); δ 6.97(s, 1H); δ 6.87 (d, *J* = 8, 1H). ^{13}C-NMR (101 MHz, d$_6$-DMSO): δ 168.38; δ 167.81; δ 158.29; δ 134.63; δ 132.37; δ 130.78; δ 123.78; δ 121.73; δ 118.14; δ 116.32. MS (ESI$^-$) m/z: 220 [M-H]$^-$.

(Z)-5-(4-hydroxybenzylidene)thiazolidine-2,4-dione (7). The title compound **7** was obtained as a yellow solid, according to general procedure using 4-hydroxybenzaldehyde (**7a**). Yield 69%. ^{1}H-NMR (401 MHz, d$_6$-DMSO): δ 12.42 (br s, exch, 1H); δ 10.28 (s, exch, 1H); δ 7.69 (s, 1H); δ 7.45 (s, 1H); δ 6.91 (s, 1H). ^{13}C-NMR (101 MHz, d$_6$-DMSO): δ 168.48; δ 167.94; δ 160.30; δ 132.79; δ 132.70; δ 124.36; δ 119.43; δ 116.73. MS (ESI$^-$) m/z: 220 [M-H]$^-$.

*(*Z)-5-(2-hydroxy-4-methoxybenzylidene)thiazolidine-2,4-dione (8).** The title compound **8** was obtained as a yellow solid, according to general procedure using 2-hydroxy-4-methoxybenzaldehyde (**8a**). Yield 75%. ^{1}H-NMR (401 MHz, d$_6$-DMSO): δ 12.39 (br s, exch, 1H); δ 10.64 (s, exch, 1H); δ 7.98 (s, 1H); δ 7.27 (d, *J* = 8.8, 1H); δ 6.59 (dd, *J* = 8.8, 2.5, 1H); δ 6.51 (d, *J* = 2.5, 1H); δ 3.77 (s, 3H). ^{13}C-NMR (101 MHz, d$_6$-DMSO): δ 168.24; δ 167.63; δ 162.66; δ 159.13; δ 129.72; δ 126.96; δ 118.38; δ 113.07; δ 106.56; δ 101.13; δ 55.32. MS (ESI$^+$) m/z: 274 [M+Na]$^+$.

(Z)-5-(4-hydroxy-3-methoxybenzylidene)thiazolidine-2,4-dione (9). The title compound **9** was obtained as a light yellow solid, according to general procedure using 4-hydroxy-3-

methoxybenzaldehyde (**9a**). Yield 62%. ^{1}H-NMR (401 MHz, d$_6$ -DMSO): δ 12.43 (br s, exch, 1H); δ 9.90 (s, exch, 1H); δ 7.71 (s, 1H); δ 7.17 (s, 1H); δ 7.08-7.05 (m, 1H); δ 6.94-6.90 (m, 1H); δ 3.83 (s, 3H). ^{13}C-NMR (101 MHz, d$_6$ -DMSO): δ 168.51; δ 167.99; δ 149.84; δ 148.40; δ 132.96; δ 124.83; δ 124.54; δ 119.73; δ 116.60; δ 114.58; δ 56.07. MS (ESI$^-$) m/z: 250 [M-H]$^-$.

(Z)-5-(4-hydroxy-3-nitrobenzylidene)thiazolidine-2,4-dione (10). The title compound **10** was obtained as a light yellow solid, according to general procedure using 4-hydroxy-3-nitrobenzaldehyde (**10a**). Yield 79%. ^{1}H-NMR (401 MHz, d$_6$ -DMSO): δ 8.14 (d, J = 2.3 Hz, 1H); δ 7.76 (s, 1H); δ 7.72 (dd, J = 8.8, 2.3 Hz, 1H); δ 7.22 (d, J = 8.8 Hz, 1H). ^{13}C-NMR (101 MHz, d$_6$ -DMSO): δ 168.88; δ 168.61; δ 155.86; δ 137.81; δ 135.78; δ 130.09; δ 128.19; δ 123.16; δ 122.55; δ 121.57. MS (ESI$^-$) m/z: 265 [M-H]$^-$.

(Z)-5-(2-fluorobenzylidene)thiazolidine-2,4-dione (11). The title compound **11** was obtained as a pale yellow solid, according to general procedure using 2-fluorobenzaldehyde (**11a**). Yield 49%. ^{1}H-NMR (401 MHz, d$_6$ -DMSO): δ 12.73 (br s, 1H); δ 7.79 (s, 1H); δ 7.56 (t, J = 6.9, 2H); δ 7.39 (t, J = 8.3, 2H). ^{13}C-NMR (101 MHz, d$_6$ -DMSO): δ 168.05; δ 167.51; δ 160.93; δ 129.24; δ 126.81; δ 125.85; δ 123.10; δ 121.36; δ 116.66. MS (ESI$^+$) m/z: 246 [M+Na]$^+$.

(Z)-5-(3-fluorobenzylidene)thiazolidine-2,4-dione (12). The title compound **12** was obtained as a yellow solid, according to general procedure using 3-fluorobenzaldehyde (**12a**). Yield 60%. ^{1}H-NMR (401 MHz, d$_6$ -DMSO): δ 12.73 (br s, 1H); δ 7.83 (s, 1H); δ 7.62 (dd, J = 14.5, 7.5, 1H); δ 7.48 (t, J = 9.9, 2H); δ 7.37 (t, J = 8.5, 1H). ^{13}C-NMR (101 MHz, d$_6$ -DMSO): δ 167.67; δ 167.27; δ 162.28; δ 135.46; δ 131.41; δ 130.32; δ 125.56; δ 125.37; δ 117.19; δ 116.74. MS (ESI$^-$) m/z: 222 [M-H]$^-$.

(Z)-5-(4-fluorobenzylidene)thiazolidine-2,4-dione (13). The title compound **13** was obtained as a yellow solid, according to general procedure using 4-fluorobenzaldehyde (**13a**). Yield 76%. ^{1}H-NMR (401 MHz, d$_6$ -DMSO): δ 12.63 (br s, exch, 1H); δ 7.81 (s, 1H); δ 7.67 (m, 2H); δ 7.39 (t, J =

8.7, 2H). ^{13}C-NMR (101 MHz, d$_6$-DMSO): δ 167.79; δ 167.32; δ 162.86; δ 132.48; δ 130.70; δ 129.74; δ 123.31; δ 116.51. MS (ESI⁻) m/z: 222 [M-H]⁻.

(Z)-5-(2-(dimethylamino)benzylidene)thiazolidine-2,4-dione (14). The title compound **14** was obtained as a yellow solid, according to general procedure using 2-(N,N-dimethylamino)benzaldehyde (**14a**). Yield 70%. ^{1}H-NMR (401 MHz, d$_6$-DMSO): δ 12.45 (br s, exch, 1H); δ 7.86 (s, 1H); δ 7.43 (dd, *J* = 12.9, 7.3, 2H); δ 7.18 (d, *J* =8.1, 1H); δ 7.10 (t, *J* = 7.5, 1H); δ 2.68 (s, 6H). ^{13}C-NMR (101 MHz, d$_6$-DMSO): δ 168.65; δ 167.88; δ 153.28; δ 131.38; δ 130.53; δ 129.83; δ 125.65; δ 122.82; δ 122.08; δ 118.81; δ 44.15. MS (ESI⁻) m/z: 247 [M-H]⁻.

(Z)-5-(3-(dimethylamino)benzylidene)thiazolidine-2,4-dione (15). The title compound **15** was obtained as a yellow solid, according to general procedure using 3-(N,N-dimethylamino)benzaldehyde (**15a**). Yield 78%. ^{1}H-NMR (401 MHz, d$_6$-DMSO): δ 12.55 (br s, exch, 1H); δ 7.73 (s, 1H); δ 7.31 (t, *J* = 7.9, 1H); δ 6.87-6.81 (m, 3H); δ 2.93 (s, 6H). ^{13}C-NMR (101 MHz, d$_6$-DMSO): δ 168.45; δ 167.74; δ 151.06; δ 134.00; δ 133.51; δ 130.16; δ 123.16; δ 117.73; δ 114.79; δ 113.99; δ 40.33. MS (ESI⁻) m/z: 247 [M-H]⁻.

(Z)-5-(4-(dimethylamino)benzylidene)thiazolidine-2,4-dione (16). The title compound **16** was obtained as an orange solid, according to general procedure using 4-(N,N-dimethylamino)benzaldehyde (**16a**). Yield 88%. ^{1}H-NMR (401 MHz, d$_6$-DMSO): δ 12.29 (br s, exch, 1H); δ 7.66 (s, 1H); δ 7.42 (d, *J* = 8.9, 2H); δ 6.81 (d, *J* = 9, 2H); δ 3.01 (s, 6H). ^{13}C-NMR (101 MHz, d$_6$-DMSO): δ 168.10; δ 167.52; δ 151.42; δ 132.83; δ 132.06; δ 119.80; δ 115.71; δ 112.01; δ 30.63. MS (ESI⁻) m/z: 247 [M-H]⁻.

(Z)-5-(pyridin-2-ylmethylene)thiazolidine-2,4-dione (17). The title compound **17** was obtained as a yellow solid, according to general procedure using 2-pyridinecarbaldehyde (**17a**). Yield 55%. ^{1}H-NMR (401 MHz, d$_6$-DMSO): δ 12.43 (br s, 1H); δ 8.75 (d, *J* = 4.7, 1H); δ 7.93 (t, *J* = 7.6, 1H); δ 7.86-7.82 (m, 2H); δ 7.42 (dd, *J* = 6.7, 5.6, 1H). ^{13}C-NMR (101 MHz, d$_6$-DMSO): δ 172.13; δ

167.55; δ 151.33; δ 149.44; δ 137.61; δ 128.12; δ 127.88; δ 127.83; δ 124.03. MS (ESI⁻) m/z: 205 [M-H]⁻.

(Z)-5-(pyridin-3-ylmethylene)thiazolidine-2,4-dione (18). The title compound **18** was obtained as a pale yellow solid, according to general procedure using 3-pyridinecarbaldehyde (**18a**). Yield 34%. ¹H-NMR (401 MHz, d₆ -DMSO): δ 12.68 (br s, 1H); δ 8.80 (s, 1H); δ 8.59 (d, J = 4.7, 1H); δ 7.93 (d, J = 8.1, 1H); δ 7.80 (s, 1H); δ 7.52 (d, J = 5.6, 1H). ¹³C-NMR (101 MHz, d₆ -DMSO): δ 167.57; δ 167.20; δ 151.31; δ 150.53; δ 135.98; δ 129.24; δ 128.38; δ 126.02; δ 124.23. MS (ESI⁻) m/z: 205 [M-H]⁻.

(Z)-5-(pyridin-4-ylmethylene)thiazolidine-2,4-dione (19). The title compound **19** was obtained as a pale pink solid, according to general procedure using 4-pyridinecarbaldehyde (**19a**). Yield 59%. ¹H-NMR (401 MHz, d₆ -DMSO): δ 12.79 (br s, 1H); δ 8.72 (d, J = 5.1, 2H); δ 7.75 (s, 1H); δ 7.54 (d, J = 5.2, 2H). ¹³C-NMR (101 MHz, d₆ -DMSO): δ 167.82; δ 167.71; δ 150.81; δ 149.72; δ 140.50; δ 128.65; δ 123.59. MS (ESI⁻) m/z: 205 [M-H]⁻.

(Z)-5-(furan-2-ylmethylene)thiazolidine-2,4-dione (20). The title compound **20** was obtained as a brown solid, according to general procedure using 2-furaldehyde (**20a**). Yield 65%. ¹H-NMR (401 MHz, d₆ -DMSO): δ 12.44 (br s, exch, 1H); δ 8.05 (s, 1H); δ 7.61 (d, J = 5.3, 1H); δ 7.09 (d, J = 3.5 1H); δ 6.76-6.75 (m, not resolved, 1H). ¹³C-NMR (101 MHz, d₆ -DMSO): δ 168.59; δ 167.05; δ 149.21; δ 147.46; δ 120.39; δ 118.55; δ 118.40; δ 113.48. MS (ESI⁻) m/z: 194 [M-H]⁻.

(Z)-5-(benzofuran-2-ylmethylene)thiazolidine-2,4-dione (21). The title compound **21** was obtained as a dark yellow solid, according to general procedure using 2-benzofurancarboxaldehyde (**21a**). Yield 59%. ¹H-NMR (401 MHz, d₆ -DMSO): δ 12.58 (br s, exch, 1H); δ 7.78-7.75 (m, not resolved, 2H); δ 7.70-7.67 (m, not resolved, 1H); δ 7.51 (s, 1H); δ 7.45 (dd, J = 14.0, 7.3, 1H); δ 7.33 (dd, J = 13.7, 7.0, 1H). ¹³C-NMR (101 MHz, d₆ -DMSO): δ 168.57; δ 166.97; δ 155.33; δ 150.89; δ 127.82; δ 127.11; δ 124.21; δ 123.98; δ 122.46; δ 118.54; δ 114.14; δ 111.50. MS (ESI⁻) m/z: 244 [M-H]⁻.

(Z)-5-(thiophen-2-ylmethylene)thiazolidine-2,4-dione (22). The title compound **22** was obtained as a grey solid, according to general procedure using 2-thiophenecarboxaldehyde (**22a**). Yield 92%. ^{1}H-NMR (401 MHz, d_6-DMSO): δ 12.56 (br s, exch, 1H); δ 8.06 (s, 1H); δ 8.02 (d, J = 5.0, 1H); δ 7.68 (d, J = 3.6, 1H); δ 7.30-7.28 (m, 1H). ^{13}C-NMR (101 MHz, d_6-DMSO): δ 166.99; δ 166.94; δ 137.15; δ 134.31; δ 132.89; δ 128.80; δ 125.00; δ 120.98. MS (ESI$^-$) m/z: 210 [M-H]$^-$.

(Z)-5-(benzothiophen-2-ylmethylene)thiazolidine-2,4-dione (23). The title compound **23** was obtained as a dark yellow solid, according to general procedure using benzo[b]thiophene-2-carboxaldehyde (**23a**). Yield 54%. ^{1}H-NMR (401 MHz, d_6-DMSO): δ 12.61 (br s, exch, 1H); δ 8.14 (s, 1H); δ 8.12-8.08 (m, 1H); δ 8.00-7.96 (m, 2H); δ 7.50-7.45 (m, 2H). ^{13}C-NMR (101 MHz, d_6-DMSO): δ 167.37; δ 167.34; δ 141.28; δ 138.83; δ 137.04; δ 131.29; δ 126.47; δ 125.46; δ 125.23; δ 125.02; δ 124.35; δ 122.90. MS (ESI$^-$) m/z: 260 [M-H]$^-$.

(Z)-5-(naphthalen-2-ylmethylene)thiazolidine-2,4-dione (24). The title compound **24** was obtained as a yellow solid, according to general procedure using 2-naphthaldehyde (**24a**). Yield 37%. ^{1}H-NMR (401 MHz, d_6-DMSO): δ 12.65 (br s, exch, 1H); δ 8.18 (s, 1H); δ 8.06-8.04 (m, 2H); δ 7.98-7.94 (m, 2H); δ 7.69 (d, J = 8.6, 1H); δ 7.64-7.58 (m, 2H). ^{13}C-NMR (101 MHz, d_6-DMSO): δ 168.38; δ 167.81; δ 133.68; δ 133.16; δ 132.18; δ 131.26; δ 131.06; δ 129.37; δ 129.13; δ 128.41; δ 128.13; δ 127.57; δ 126.42; δ 124.30. MS (ESI$^+$) m/z: 254 [M+Na]$^+$.

(Z)-5-(anthracen-9-ylmethylene)thiazolidine-2,4-dione (25). The title compound **25** was obtained as an orange solid, according to general procedure using anthracene-9-carbaldehyde (**25a**). Yield 18%. ^{1}H-NMR (401 MHz, CDCl$_3$): δ 8.79 (s, 1H); δ 8.55 (s, 1H); δ 8.07 (d, J = 8.2, 2H); δ 7.98 (d, J = 8.8, 2H); 7.60-7.52 (m, 4H). ^{13}C-NMR (101 MHz, CDCl$_3$): δ 166.87; δ 165.04; δ 133.38; δ 131.32; δ 131.11; δ 129.82; δ 129.41; δ 128.70; δ 127.23; δ 126.81; δ 125.89; δ 125.04. MS (ESI$^-$) m/z: 304 [M-H]$^-$.

(Z)-5-((E)-3-phenylallylidene)thiazolidine-2,4-dione (26). The title compound **26** was obtained as a pale yellow solid, according to general procedure using cinnamaldehyde (**26a**). Yield 36%. ^{1}H-

NMR (401 MHz, d_6-DMSO): δ 12.31 (br s, 1H); δ 7.67-7.65 (m, 2H); δ 7.47-7.35 (m, 4H); δ 7.27 (d, J = 15.3, 1H); δ 6.91 (dd, J = 15.3, 11.4, 1H). ^{13}C-NMR (101 MHz, d_6-DMSO): δ 168.61; δ 143.33; δ 136.07; δ 131.94; δ 130.03; δ 129.34; δ 128.13; δ 124.09; δ 109.95. MS (ESI⁻) m/z: 230 [M-H]⁻.

(Z)-5-((E)-3-(4-(dimethylamino)phenyl)allylidene)thiazolidine-2,4-dione (27). The title compound **27** was obtained as a dark red solid, according to general procedure using (E)-3-(4-(dimethylamino)phenyl)acrylaldehyde (**27a**). Yield 58%. ^{1}H-NMR (401 MHz, d_6-DMSO): δ 12.23 (br s, 1H); δ 7.47 (dd, J = 19.7, 10.2, 3H); δ 7.16 (d, J = 15.0, 1H); δ 6.72 (d, J = 8.9, 2H); δ 6.61 (dd, J = 15.0, 11.6, 1H); δ 2.99 (s, 6H). ^{13}C-NMR (101 MHz, d_6-DMSO): δ 168.23; δ 167.32; δ 151.79; δ 145.30; δ 133.96; δ 129.97; δ 123.61; δ 120.93; δ 118.50; δ 112.31; δ 40.13. MS (ESI⁻) m/z: 273 [M-H]⁻.

(Z)-5-((1H-indol-3-yl)methylene)thiazolidine-2,4-dione (28). The title compound **28** was obtained as a yellow solid, according to general procedure using 1H-indole-3-carbaldehyde (**28a**). Yield 45%. ^{1}H-NMR (401 MHz, d_6-DMSO): δ 12.29 (br s, 1H); δ 12.12 (s, exch, 1H); δ 8.06 (s, 1H); δ 7.89 (d, J = 7.8, 1H); δ 7.74 (s, 1H); δ 7.50 (d, J = 7.9, 1H); δ 7.27-7.18 (m, 2H). ^{13}C-NMR (101 MHz, d_6-DMSO): δ 168.09; δ 167.69; δ 136.62; δ 129.06; δ 127.19; δ 124.93; δ 123.49; δ 121.47; δ 118.75; δ 116.59; δ 112.82; δ 110.83. MS (ESI⁻) m/z: 243 [M-H]⁻.

(Z)-5-((5-methoxy-1H-indol-3-yl)methylene)thiazolidine-2,4-dione (29). The title compound **29** was obtained as a dark yellow solid, according to general procedure using 5-methoxy-1H-indole-3-carbaldehyde (**29a**). Yield 47%. ^{1}H-NMR (401 MHz, d_6-DMSO): δ 12.25 (br s, 1H); δ 12.00 (s, 1H); δ 8.09 (s, 1H); δ 7.66 (d, J = 3.0, 1H), δ 7.40 (dd, J = 18.0, 5.5, 2H); δ 6.86 (dd, J = 8.8, 2.3, 1H); δ 3.82 (s, 3H). ^{13}C-NMR (101 MHz, d_6-DMSO): δ 168.19; δ 167.77; δ 155.36; δ 131.43; δ 129.19; δ 128.05; δ 125.43; δ 115.76; δ 113.80; δ 113.59; δ 110.86; δ 100.47; δ 55.88. MS (ESI⁻) m/z: 273 [M-H]⁻.

(Z)-5-((5-methoxy-1-methyl-1H-indol-3-yl)methylene)thiazolidine-2,4-dione (30). The title compound **30** was obtained as an orange solid, according to general procedure using 5-methoxy-1-methyl-1H-indole-3-carbaldehyde (**30a**). Yield 44%. ^{1}H-NMR (401 MHz, d$_6$ -DMSO): δ 12.25 (br s, 1H); δ 8.07 (s, 1H); δ 7.73 (s, 1H); δ 7.52–7.44 (m, 2H); δ 6.92 (dd, J = 8.9, 2.3 Hz, 1H); δ 3.89 (s, 3H); δ 3.84 (s, 3H). ^{13}C-NMR (101 MHz, d$_6$ -DMSO): δ 168.20; δ 167.73; δ 155.68; δ 132.72; δ 132.20; δ 128.56; δ 124.96; δ 115.48; δ 113.73; δ 112.10; δ 109.72; δ 100.71; δ 55.95; δ 33.85. MS (ESI$^-$) m/z: 287 [M-H]$^-$.

(Z)-5-((1-methyl-1H-benzo[d]imidazol-2-yl)methylene)thiazolidine-2,4-dione (31). The title compound **31** was obtained as an orange solid, according to general procedure using 1-methyl-1H-benzo[d]imidazole-2-carbaldehyde (**31a**). Yield 48%. ^{1}H-NMR (401 MHz, d$_6$ -DMSO): δ 12.57 (br s, 1H); δ 7.84 (s, 1H); δ 7.75 (d, J = 8.0, 1H); δ 7.67 (d, J = 8.0, 1H); δ 7.34 (dt, J = 26.1, 7.1, 2H); δ 3.99 (s, 3H). ^{13}C-NMR (101 MHz, d$_6$ -DMSO): δ 171.21; δ 167.41; δ 147.97; δ 143.15; δ 136.28; δ 131.34; δ 124.48; δ 123.49; δ 120.04; δ 115.69; δ 111.43; δ 30.25. MS (ESI$^+$) m/z: 260 [M+Na]$^+$.

(Z)-5-((2-phenyl-1H-indol-3-yl)methylene)thiazolidine-2,4-dione (32). The title compound **32** was obtained as an orange solid, according to general procedure using 2-phenyl-1H-indole-3-carbaldehyde (**32a**). Yield 22%. ^{1}H-NMR (401 MHz, d$_6$ -DMSO): δ 12.31 (br s, 1H); δ 12.27 (s, exch 1H); δ 7.96 (s, 1H); δ 7.78 (d, J = 7.9, 1H); 7.63-7.49 (m, 6H); δ 7.29-7.19 (m, 2H). ^{13}C-NMR (101 MHz, d$_6$ -DMSO): δ 168.44; δ 142.21; δ 136.91; δ 131.44; δ 129.56; δ 129.44; δ 128.09; δ 126.01; δ 123.47; δ 121.18; δ 120.40; δ 120.28; δ 112.68; δ 107.31. MS (ESI$^-$) m/z: 319 [M-H]$^-$.

(Z)-5-([1,1'-biphenyl]-4-ylmethylene)thiazolidine-2,4-dione (33). The title compound **33** was obtained as a white solid, according to general procedure using [1,1'-biphenyl]-4-carbaldehyde (**33a**). Yield 55%. ^{1}H-NMR (401 MHz, d$_6$ -DMSO): δ 12.64 (br s, 1H); δ 7.86-7.83 (m, 3H); δ 7.72 (dd, J = 21.4, 8.0, 4H); δ 7.50 (t, J = 7.6, 2H); δ 7.41 (t, J = 7.3, 1H). ^{13}C-NMR (101 MHz, d$_6$ -DMSO): δ 168.28; δ 167.88; δ 142.15; δ 139.25; δ 132.52; δ 131.66; δ 131.10; δ 129.50; δ 128.63; δ 127.81; δ 127.21; δ 123.94. MS (ESI$^-$) m/z: 280 [M-H]$^-$.

(Z)-5-(2-(benzyloxy)benzylidene)thiazolidine-2,4-dione (34). The title compound **34** was obtained as a pale yellow solid, according to general procedure using 2-(benzyloxy)benzaldehyde (**34a**). Yield 61%. ^{1}H-NMR (401 MHz, d$_6$ -DMSO): δ 12.58 (br s, 1H); δ 8.03 (s, 1H); δ 7.48-7.42 (m, 6H); δ 7.36 (t, *J* = 6.5, 1H); δ 7.24 (d, *J* = 8.4, 1H); δ 7.11 (t, *J* = 7.5, 1H); δ 5.25 (s, 2H). ^{13}C-NMR (101 MHz, d$_6$ -DMSO): δ 168.43; δ 167.77; δ 157.61; δ 136.94; δ 132.66; δ 128.98; δ 128.81; δ 128.47; δ 128.10; δ 126.64; δ 124.02; δ 122.35; δ 121.63; δ 113.73; δ 70.35. MS (ESI$^+$) m/z: 334 [M+Na]$^+$.

(Z)-5-((2,3-dihydrobenzo[b][1,4]dioxin-6-yl)methylene)thiazolidine-2,4-dione (35). The title compound **35** was obtained as a pale yellow solid, according to general procedure using 2,3-dihydrobenzo[b][1,4]dioxine-6-carbaldehyde (**35a**). Yield 75%. ^{1}H-NMR (401 MHz, d$_6$ -DMSO): δ 12.52 (br s, 1H); δ 7.69 (s, 1H); δ 7.12–7.10 (m, 2H); δ 7.02 (dd, *J* = 7.6, 1.2, 1H); δ 4.30-4.25 (m, 4H). ^{13}C-NMR (101 MHz, d$_6$ -DMSO): δ 168.40; δ 168.01; δ 146.04; δ 144.13; δ 131.99; δ 126.78; δ 124.21; δ 121.60; δ 119.16; δ 118.42; δ 64.89; δ 64.41. MS (ESI$^-$) m/z: 262 [M-H]$^-$.

(Z)-5-((7-methoxybenzo[d][1,3]dioxol-5-yl)methylene)thiazolidine-2,4-dione (36). The title compound **36** was obtained as a yellow solid, according to general procedure using 7-methoxybenzo[d][1,3]dioxole-5-carbaldehyde (**36a**). Yield 58%. ^{1}H-NMR (401 MHz, d$_6$ -DMSO): δ 12.55 (br s, 1H); δ 7.72 (s, 1H); δ 6.97 (s, 1H); δ 6.82 (s, 1H); δ 6.11 (s, 2H); δ 3.87 (s, 3H). ^{13}C-NMR (101 MHz, d$_6$ -DMSO): δ 168.33; δ 167.98; δ 149.56; δ 143.91; δ 137.43; δ 132.28; δ 128.02; δ 122.08; δ 111.80; δ 103.44; δ 102.68; δ 56.82. MS (ESI$^-$) m/z: 278 [M-H]$^-$.

(Z)-5-((2-chloroquinolin-3-yl)methylene)thiazolidine-2,4-dione (37). The title compound **37** was obtained as a pale yellow solid, according to general procedure using 2-chloroquinoline-3-carbaldehyde (**37a**). Yield 45%. ^{1}H-NMR (401 MHz, d$_6$ -DMSO): δ 12.87 (br s, 1H); δ 8.55 (s, 1H); δ 8.24 (d, *J* = 8.1, 1H); δ 8.00-7.88 (m, 3H); δ 7.73 (t, *J* = 7.2, 1H). ^{13}C-NMR (101 MHz, d$_6$ -DMSO): δ 167.91; δ 167.26; δ 149.81; δ 146.90; δ 138.45; δ 132.88; δ 129.42; δ 128.63; δ 128.11; δ 126.92; δ 126.29; δ 125.85. MS (ESI$^-$) m/z: 290 [M-H]$^-$.

(Z)-5-((2-chloro-6-methoxyquinolin-3-yl)methylene)thiazolidine-2,4-dione (38). The title compound **38** was obtained as a yellow solid, according to general procedure using 2-chloro-6-methoxyquinoline-3-carbaldehyde (**38a**). Yield 32%. ^{1}H-NMR (401 MHz, d_6 -DMSO): δ 12.85 (br s, 1H); δ 8.44 (s, 1H); δ 7.94 (s, 1H); δ 7.89 (d, $J = 9.2$, 1H); δ 7.69 (d, $J = 2.5$, 1H); δ 7.52 (dd, $J = 9.1, 2.7$, 1H); δ 3.92 (s, 3H). ^{13}C-NMR (101 MHz, d_6 -DMSO): δ 167.96; δ 167.33; δ 158.75; δ 147.17; δ 142.93; δ 137.08; δ 129.52; δ 129.19; δ 128.33; δ 126.21; δ 125.88; δ 125.19; δ 107.20; δ 56.26. MS (ESI⁻) m/z: 320 [M-H]⁻.

Biology

Inhibition of GSK-3β (Kinase-Glo). Human recombinant GSK-3β was purchased from Millipore (Millipore Iberica S.A.U.). The prephoshorylated polypeptide substrate was purchased from Millipore (Millipore Iberica SAU). Kinase-Glo Luminescent Kinase Assay was obtained from Promega (Promega Biotech Iberica, SL). ATP and all other reagents were from Sigma-Aldrich (St. Louis, MO). Assay buffer contained 50 mM HEPES (pH 7.5), 1 mM EDTA, 1 mM EGTA, and mM magnesium acetate. The method of Baki et al.[67] was followed analyze the inhibition of GSK-3β. Kinase-Glo assays were performed in assay buffer using white 96-well plates. In a typical assay, 10 μL (10 μM) of the tested compound (dissolved in DMSO at mM concentration and diluted in advance in assay buffer to the desired concentration) and 10 μL (20 ng) of enzyme were added to each well followed by 20 μL of assay buffer containing 25 μM substrate (GS-2 peptide) and 1 μM ATP. The final DMSO concentration in the reaction mixture did not exceed 1%. After a 30 min incubation at 30 °C, the enzymatic reaction was stopped with 40 μL of Kinase-Glo reagent. Glow-type luminescence was recorded after 10 min using a Fluoroskan Ascent multimode reader. The activity is proportional to the difference of the total and consumed ATP. The inhibitory activities were calculated on the basis of maximal kinase and luciferase activities measured in the absence of inhibitor and in the presence of a reference compound inhibitor (TDZD8, Sigma Aldrich, IC$_{50}$ =

0.69 μM) at total inhibition concentration, respectively. The linear regression parameters were determined and the IC_{50} extrapolated (GraphPad Prism 4.0, GraphPad Software Inc.).

Mechanism of action on GSK3β. Kinetic studies. To investigate the inhibitory mechanism of **28** and **30** on GSK-3β, kinetic experiments were performed. Lineweaver−Burk plots of enzyme kinetics are shown in Kinetic experiments varying both ATP (from 1 to 50 μM) and inhibitor concentrations were performed. Double-reciprocal plotting of the data is depicted in Figure 4. The intercept of the plot in the vertical axis (1/V) does not change when the inhibitors concentration increases. These results would suggest that inhibitors act as competitive inhibitors of ATP binding.

Inhibition of GSK-3β (TR-FRET). The assays were performed in white Optiplate-384 at room temperature (22 °C) in a final volume of 25 μL, using the following Kinase Buffer: 50 mM HEPES pH 7.5, 1 mM EGTA, 10 mM $MgCl_2$, 2 mM DTT and 0.01% Tween-20. The compounds were dissolved in DMSO and then diluted in Kinase Buffer, keeping constant the concentration of DMSO (3%) in each well. In each assay, the compound SB216763 was used as positive control (IC_{50} 11.4±2.1 nM), while DMSO was used as reference. GSK-3β (0.5 nM, final concentration) was first incubated with the two compounds for 30 minutes, then a mixture of ATP (10 μM, final concentration) and U*Light*-GS (Ser641/pSer657) Peptide (50 nM, final concentration) was added. The reaction was incubated for 1 h, afterwards the kinase reaction was stopped by adding 24 mM EDTA and 2 nM (final concentration) of Eu-anti-phospho-GS (Ser641) antibody, both diluted in Detection Buffer 1X. After an incubation of 1 h, the TR-FRET signal was read with the EnSight Multimode Plate Reader (excitation at 320 nm and emissions at 615 and 665 nm). The compounds were tested in 10-dose IC_{50} mode with two-fold serial dilutions. Data were analysed using Excel and GraphPad Prism software (version 6.0, GraphPad) for IC_{50} curve fits using sigmoidal dose-response (variable slope) equation. Values obtained for each compound are the means ± SD determined for at least two separate experiments. Compounds **28** and **30** are soluble in the assay conditions as determined at the maximum concentration tested (nephelometry determination) and

do not interfere with the readout of the assay (no absorption at 320 nm and no emission at 615 and 665 nm).

Inhibition of casein kinase 1 (CK1) δ and ε. Human recombinant CK1δ and CK1ε was purchased from Millipore (Millipore Iberica S.A.U.). Casein solution from bovine milk, 5%, was purchased from Sigma-Aldrich (St. Louis, MO). ATP and all other reagents were from Sigma-Aldrich (St. Louis, MO). Assay buffer contained 50 mM HEPES, pH 7,5; 0,01% Brij-35; 10 mM Cl_2Mg; 1 mM EGTA and 0,01 % NaN_3. Kinase-Glo Kit from Promega was used to test compounds **28** and **30** for activity against CK-1. The Kinase-Glo assays were performed in the above mentioning assay buffer using black 96-well plates. Typically, 10 µL of test compound (dissolved in DMSO at 1 mM concentration and diluted in advance in assay buffer to 10 µM) and 10 µL (16 ng) of enzyme were added to each well followed by 20 µL of assay buffer containing 0.1% casein as substrate and 4 µM ATP. The final DMSO concentration in the reaction mixture did not exceed 1%. After 60 min incubation at 30 °C the enzymatic reaction was stopped with 40 µL of Kinase-Glo reagent. Glow-type luminescence was recorded after 10 min using a FLUOstar Optima (BMG Labtechnologies GmbH, Offenburg, Germany) multimode reader. The activity is proportional to the difference of the total and consumed ATP. The inhibitory activities were calculated on the basis of maximal activities measured in the absence of inhibitor. The IC_{50} was defined as the concentration of each compound that reduces a 50% the enzymatic activity with respect to that without inhibitors. Each value is the mean of two independent experiments.

Inhibition of cell division cycle 7 (Cdc7). The ADP-Glo^{TM} Kinase Assay + CDC7 / DBF4 Kinase Enzyme System (no. catalog V5089) from Promega was used to screen compounds for activity against CDC7. ATP and other reagents were purchased from Sigma-Aldrich (St. Louis, MO). The assays were performed in a buffer solution using 96-well plates. Compounds **28** and **30** (5 µL, 40 µM dissolved in 4% DMSO) was added to each well followed by the enzyme (5 µL, 25 ng / well), ATP (5 µL, final concentration in the well 10 µM) and PDKtidE (5 µL, 4 µg / well) as substrate. Then it was allowed to incubate for 60 min at room temperature and ADP-Glo™ reagent (20 µL)

was added allowing to incubate again for 40 min at room temperature. Behind the incubation, the kinase detection agent (40 μL) was added and allowed to incubate for 30 min at room temperature. Finally, the luminescence was recorded using a FLUOstar Optima (BMG Labtechnologies GmbH, Offenburg, Germany) multimode reader. The inhibition activities were calculated based on the maximum activity, measured in the absence of inhibitor.

Blood Brain Barrier permeation. Prediction of the brain penetration was evaluated using a PAMPA-BBB.[70] Ten commercial drugs, phosphate buffer saline solution at pH 7.4 (PBS), ethanol and dodecane were purchased from Sigma Aldrich, Acros organics, Merck, and Fluka. The porcine polar brain lipid (PBL) (catalog no. 141101) was from Avanti Polar Lipids. The donor plate was a 96-well filtrate plate (Multiscreen® IP Sterile Plate PDVF membrane, pore size is 0.45 μM, catalog no. MAIPS4510) and the acceptor plate was an indented 96-well plate (Multiscreen®, catalog no. MAMCS9610) both from Millipore. Filter PDVF membrane units (diameter 30 mm, pore size 0.45 μm) from Symta were used to filter the samples. A 96-well plate UV reader (Thermoscientific, Multiskan spectrum) was used for the UV measurements. Test compounds [(3-5 mg of Caffeine, Enoxacine, Hydrocortisone, Desipramine, Ofloxacine, Piroxicam, Testosterone), (12 mg of Promazine) and 25 mg of Verapamil and Atenolol] were dissolved in EtOH (1000 μL). 100 μL of this compound stock solution was taken; 1400 μL of EtOH and 3500 μL of PBS pH =7.4 buffer were then added to reach 30% of EtOH concentration in the experiment. These solutions were filtered. The acceptor 96-well microplate was filled with 180 μL of PBS/EtOH (70/30). The donor 96-well plate was coated with 4 μL of porcine brain lipid in dodecane (20 mg/mL) and after 5 minutes, 180 μL of each compound solution was added. 1-2 mg of each compound were dissolved in 1500 μL of EtOH and 3500 μL of PBS pH =7.4 buffer, filtered and then added to the donor 96-well plate to be determined their ability to pass the brain barrier. Then the donor plate was carefully put on the acceptor plate to form a "sandwich", which was left undisturbed for 2h and 30 min at 25°C. During this time the compounds diffused from the donor plate through the brain lipid membrane into the acceptor plate. After incubation, the donor plate was removed. UV plate reader

determined the concentration of compounds and commercial drugs in the acceptor and the donor wells. Every sample was analyzed at three to five wavelengths, in 3 wells and in two independent runs. Results are given as the mean [standard deviation (SD)] and the average of the two runs is reported. Ten quality control compounds (previously mentioned) of known BBB permeability were included in each experiment to validate the analysis set.

Neuro- and hepato-toxicity assessment. Primary cultures of CGNs were prepared from 7 day-old pups of the same rat strain, as previously described.[98, 99] All animal experiments were authorized by the University of Bologna bioethical committee (Protocol n° 17-72-1212) and performed according to Italian and European Community laws on the use of animals for experimental purposes. For cerebellar granule cultures, cells were dissociated from cerebella and plated on 96 well plates, previously coated with 10 μg/mL poly-L-lysine, at a density of 3×105 cells/0.2 mL medium/well in BME supplemented with 100 mL/L heat-inactivated FBS (Life technologies), 2 mM glutamine, 100 μM gentamicin sulphate and 25 mM KCl (all from Sigma-Aldrich). 16 h later, 10 μM cytosine arabino-furanoside (Sigma-Aldrich) was added to avoid glial proliferation. After 7 days in vitro, differentiated neurons were shifted to serum free BME medium containing 25 mM KCl without serum and different treatments were performed.

HepG2 cells (human hepatocellular liver carcinoma cell line from American Type Culture Collection, ATCC), were grown in DMEM supplemented with 10% FBS and 50 units/mL of penicillin/ streptomycin (Life Technologies) at 37 °C in a humidified atmosphere containing 5% CO_2. For the experiments, cells (0.5×105 cells/well) were seeded in 96-well plate in complete medium; after 24 h, the medium was removed, and cells were exposed to the increasing concentrations of previously selected non-neurotoxic compounds (0, 10, 25, and 50 μM) in DMEM with no serum for further 24 h and survival was measured through MTT assay.

The viability of the different cell types (CGNs and HepG2) exposed to increasing concentrations of the studied compounds (0, 5, 25 and 50 μM) for 24 h was evaluated through the MTT assay. Briefly, thiazolyl blue was added to the culture medium at a final concentration of 0.1 mg/mL.

Following a 20 min incubation for CGNs and 10 min for HepG2 cells at 37 °C in the dark, the MTT precipitate was dissolved in 0.1 M Tris-HCl pH 7.5 buffer containing 5% Triton X-100 (all from Sigma-Aldrich) and absorbance was read at 570 nm in a multiplate spectophotometric reader (Bio-Rad).

AcPHF6 aggregation and inhibition studies by ThT fluorescence. ThT fluorescence assays were performed as described previously by Lunven *et al.*[79] with some variations. AcPHF6 (Celtek Peptides) was initially dissolved in 1,1,1,3,3,3,-hexafluoro-2-propanol, kept at room temperature overnight, aliquoted and dried. Stock solutions of AcPHF6 (0.5 mM) were then prepared in ultrapure water immediately prior to fluorescence assays. Stock solutions of all tested compounds (2 mM) were prepared in DMSO, while stock solution of ThT (0.5 mM) was prepared in 50 mM phosphate buffer pH 7.4. AcPHF6 aggregation was monitored using standard 96-well plates and an EnSpire plate reader (PerkinElmer) setting the excitation and emission wavelengths at 446 and 490 nm, respectively. Samples were prepared by diluting stock solutions in 50 mM phosphate buffer pH 7.4 to a final AcPHF6 concentration of 50 μM with 20 μM ThT and 10 μM test compound (maximum final DMSO content: 0.5%, v/v); the final volume was 100 μL. Assays were performed at 25°C. Fluorescence data were recorded every minute over 120 min with 10 s shaking (400 rpm) prior to each reading. Each condition was assayed at least in triplicate and values were averaged. Estimation of the inhibitory potency (%) was carried out by comparing fluorescence values at the plateau (average fluorescence intensity value in the 70-80 min range).

CD spectroscopy. CD spectra were measured in the 260–200 nm spectral range on a Jasco J-810 spectropolarimeter (Tokyo, Japan) equipped with a PTC-423S Peltier-type temperature control system. Measurements were carried out at 25 °C using quartz cells with 1 mm pathlength (Hellma, Milan, Italy), a 50 nm min^{-1} scanning speed, a 2 nm response, a 2 nm spectral bandwidth and an accumulation cycle of 3. Stock solutions of AcPHF6 (1 mM) were prepared in water immediately prior to CD measurements, while stock solutions of compounds **28** and **30** (2 mM) were prepared in methanol/DMSO (95:5, v/v). Samples were prepared by diluting stock solutions in phosphate buffer

50 mM (pH 7.4) to a final AcPHF6 concentration of 100 μM with 20 μM test compound (final DMSO content: 0.05%, v/v). The spectral contribution of solvents and test compounds was subtracted to derive the CD spectra of AcPHF6, then data were converted to molar units per residue ($\Delta\varepsilon_\mathrm{res}$) and plotted using the Bezier smoothing algorithm provided by the Gnuplot software (version 5.2.2, http://gnuplot.sourceforge.net).

Atomic force microscopy. Atomic Force Microscopy imaging was performed in PeakForce™ tapping-mode on a Nanoscope Multimode 8 (Bruker, U.S.A.) with ScanAsyst Air probes (Bruker). Peptide specimens were prepared by quickly diluting a freshly- prepared 500 μM aliquot of AcPHF6 peptide in water to 50 μM concentration in 50 mM phosphate buffer (pH 7.4) or in the same buffer additionally containing 10 μM of either compound **28** or **30**, briefly vortexing and then subjecting the specimens to the same incubation procedure detailed for ThT fluorescence measurements (briefly, incubation at 25°C for 80 min with 400 rpm shaking for 10 s every minute). At the end of the incubation, the peptide solutions were immediately filtered through Microcon centrifuge ultrafiltration devices (MWCO 30 kDa, Millipore) to separate the small MW fraction from the polymerized peptide fraction. Additional runs on the same Microcons were performed in order to exchange the different buffers with ultrapure water. 5 μL aliquots of the high-molecular weight retentate fractions were layered on discs of freshly cleaved muscovite mica (EMS, U.S.A.) and allowed to dry while protected from ambient contamination. The recorded micrographs were only processed by flattening with Bruker's Nanoscope Analysis software (version 1.8).

K18 aggregation and inhibition studies. K18 aggregations were performed in a black 96-well optical flat bottom plate (Thermoscientific) with a basic reaction mix (BRM) prepared as follow: 21 μM K18, heparin 0.015 mg/mL, 0.1 mM DTT, 10 μM ThT in PBS 1X. Five different experimental conditions were assessed: (1) BRM alone to assess the kinetic of tauK18 self-assembly; BRM supplemented with **30** at the final concentration of (2) 1 μM; (3) 5 μM; and (4) 10 μM; (5) BRM supplemented with 1% DMSO. Each experimental condition was prepared and analyzed in triplicate. The plate was sealed with a sealing film, inserted into a FLUOstar OPTIMA microplate

reader (BMG Labtech) and subjected to cycles of shaking (1 minute at 300 rpm - double orbital) and incubation (14 minutes) at 37°C. Fluorescence readings (480 nm) were taken every 15 minutes (30 flashes per well at 450 nm).

Full-length 2N4R tau aggregation and inhibition studies. TauFL 2N4R aggregation was performed in a black 96-well optical flat bottom plate (Thermoscientific) with a basic reaction mix (BRM) prepared as follow : 20 µM tauFL (2N4R), heparin 0.02 mg/mL, 0.5 mM DTT, 10 µM ThT in PBS 1X. Three different experimental conditions were assessed: (1) BRM alone to assess the kinetic of TauFL 2N4R self-assembly; (2) BRM supplemented with **30** at the final concentration of 10 µM; (3) BRM supplemented with 1% DMSO was used as control for the reaction. The plate was then inserted into a FLUOstar OPTIMA microplate reader (BMG Labtech) and subjected to cycles of shaking (1 minute at 600 rpm – single orbital) and incubation (1 minute) at 42°C. Fluorescence readings (480 nm) were taken every 2 minutes (100 flashes per well at 450 nm).

Okadaic acid-induced tau hyperphosphorylation cell model. Human SH-SY5Y cells were grown in DMEM supplemented with 10% FBS and 1% penicillin-streptocycin at 37 ºC and 5% CO_2 in an incubator. SH-SY5Y cells were seeded onto 96-well plate at 60000 cells per well. 48 hours later, cells were pre-incubated with the compounds at the desired concentration for 1 hour and after that time OA (acquired from Sigma Aldrich, catalogue number: 09381) was added at a concentration of 30nM and incubated for another 24 hours. Afterwards, cells were incubated with 0.5mg/mL MTT solution for at least 4 hours at 37 ºC and 5% CO_2. Then culture media was removed and the formazan crystals attached to the bottom of the plate were dissolved with 200µL of DMSO. Finally, UV-absorbance was measured at 595nM in a microplate reader (Varioskan Flash Microplate reader, Thermo Scientific).

SUPPORTING INFORMATION

The Supporting Information is available free of charge on the ACS Publications website.

Retrospective computational studies; PAMPA-BBB assay data; Jump dilution assay; synthetic details for compounds **14a** and **15a**; compounds purity by HPLC; ^{1}H- and ^{13}C- NMR spectra of all synthesized compounds.

Molecular Formula Strings and GSK-3β data.

AUTHOR INFORMATION

Corresponding Author

*E-mail, marialaura.bolognesi@unibo.it; phone +39 0512099717

ORCID

0000-0002-1289-5361

NOTES

The authors declare no competing financial interest.

ABBREVIATIONS USED

Aβ, amyloid β; AD, Alzheimer's disease; AFM, atomic force microscopy; ATP, adenosine 5'-triphosphate; BBB, blood-brain barrier; CD, Circular dichroism; Cdc7, cell division cycle 7; CGNs, cerebellar granule neurons; CK1, casein kinase 1; CNS, central nervous system; EDDA, ethylenediamine diacetate; GSK-3β, glycogen synthase kinase 3β; HepG2, human hepatoma cell line; MAP, microtubule-associated protein; MTDLs, multi-target directed ligands; MTT, 3-(4,5-

dimethylthiazol-2-yl)-2,5-diphenyltetrazolium bromide; MW, microwave; NFTs, neurofibrillary tangles; OA, okadaic acid; PAINS, Pan Assay Interference Compounds; PAMPA, Parallel Artificial Membrane Permeability Assay; P_e, effective permeability; PIO, pioglitazone; RT-QuIC, Real-Time Quaking-Induced Conversion; SAR, structure-activity relationship; TDZDs, thiadiazolidinediones; ThT, thioflavin T; TR-FRET, Time-Resolved Fluorescence Energy Transfer; TZD, 2,4-thiazolidinedione.

References

1.   Cummings, J. L.; Morstorf, T.; Zhong, K. Alzheimer's disease drug-development pipeline: few candidates, frequent failures. *Alzheimers Res Ther* **2014,** 6, 37.

2.   Uliassi, E.; Gandini, A.; Perone, R. C.; Bolognesi, M. L. Neuroregeneration versus neurodegeneration: toward a paradigm shift in Alzheimer's disease drug discovery. *Future Med Chem* **2017,** 9, 995-1013.

3.   Dolsten, M. Learn more about our neuroscience R&D decision. https://www.pfizer.com/news/featured_stories/featured_stories_detail/learn_more_about_our_neuro science_r_d_decision (05 February 2018).

4.   Mattson, M. P. Pathways towards and away from Alzheimer's disease. *Nature* **2004,** 430, 631.

5.   Iqbal, K.; Grundke-Iqbal, I. Alzheimer Disease, a Multifactorial Disorder Seeking Multi-therapies. *Alzheimer's & dementia : the journal of the Alzheimer's Association* **2010,** 6, 420-424.

6.   Viayna, E.; Sola, I.; Di Pietro, O.; Munoz-Torrero, D. Human disease and drug pharmacology, complex as real life. *Curr Med Chem* **2013,** 20, 1623-34.

7.   Youdim, M. B.; Buccafusco, J. J. Multi-functional drugs for various CNS targets in the treatment of neurodegenerative disorders. *Trends Pharmacol Sci* **2005,** 26, 27-35.

8.   Hopkins, A. L. Network pharmacology: the next paradigm in drug discovery. *Nat Chem Biol* **2008,** 4, 682-90.

9.		Cavalli, A.; Bolognesi, M. L.; Minarini, A.; Rosini, M.; Tumiatti, V.; Recanatini, M.; Melchiorre, C. Multi-target-directed ligands to combat neurodegenerative diseases. *J Med Chem* **2008,** 51, 347-72.

10.		Bajda, M.; Guzior, N.; Ignasik, M.; Malawska, B. Multi-target-directed ligands in Alzheimer's disease treatment. *Curr Med Chem* **2011,** 18, 4949-75.

11.		Leon, R.; Garcia, A. G.; Marco-Contelles, J. Recent advances in the multitarget-directed ligands approach for the treatment of Alzheimer's disease. *Med Res Rev* **2013,** 33, 139-89.

12.		Dias, K. S.; Viegas, C., Jr. Multi-Target Directed Drugs: A Modern Approach for Design of New Drugs for the treatment of Alzheimer's Disease. *Curr Neuropharmacol* **2014,** 12, 239-55.

13.		Prati, F.; Cavalli, A.; Bolognesi, M. L. Navigating the Chemical Space of Multitarget-Directed Ligands: From Hybrids to Fragments in Alzheimer's Disease. *Molecules* **2016,** 21, 466.

14.		Hardy, J. A.; Higgins, G. A. Alzheimer's disease: the amyloid cascade hypothesis. *Science* **1992,** 256, 184-5.

15.		Wolfe, M. S. Introduction to special issue on Alzheimer's disease. *J Med Chem* **2012,** 55, 8977-8.

16.		Yuan, J.; Venkatraman, S.; Zheng, Y.; McKeever, B. M.; Dillard, L. W.; Singh, S. B. Structure-Based Design of β-Site APP Cleaving Enzyme 1 (BACE1) Inhibitors for the Treatment of Alzheimer's Disease. *Journal of Medicinal Chemistry* **2013,** 56, 4156-4180.

17.		Prati, F.; Bottegoni, G.; Bolognesi, M. L.; Cavalli, A. BACE-1 Inhibitors: From Recent Single-Target Molecules to Multitarget Compounds for Alzheimer's Disease. *J Med Chem* **2018,** 61, 619-637.

18.		Abbott, A. Neuroscience: The plaque plan. *Nature* **2008,** 456, 161-4.

19.		Oehlrich, D.; Berthelot, D. J. C.; Gijsen, H. J. M. γ-Secretase Modulators as Potential Disease Modifying Anti-Alzheimer's Drugs. *Journal of Medicinal Chemistry* **2011,** 54, 669-698.

20.		Herrup, K. The case for rejecting the amyloid cascade hypothesis. *Nat Neurosci* **2015,** 18, 794-9.

21.   Hawkes, N. Merck ends trial of potential Alzheimer's drug verubecestat. *Bmj* **2017,** 356, j845.

22.   Doig, A. J.; Del Castillo-Frias, M. P.; Berthoumieu, O.; Tarus, B.; Nasica-Labouze, J.; Sterpone, F.; Nguyen, P. H.; Hooper, N. M.; Faller, P.; Derreumaux, P. Why Is Research on Amyloid-beta Failing to Give New Drugs for Alzheimer's Disease? *ACS Chem Neurosci* **2017,** 8, 1435-1437.

23.   Villemagne, V. L.; Fodero-Tavoletti, M. T.; Masters, C. L.; Rowe, C. C. Tau imaging: early progress and future directions. *Lancet Neurol* **2015,** 14, 114-24.

24.   Li, C.; Götz, J. Tau-based therapies in neurodegeneration: opportunities and challenges. *Nature Reviews Drug Discovery* **2017,** 16, 863.

25.   Ballatore, C.; Lee, V. M. Y.; Trojanowski, J. Q. Tau-mediated neurodegeneration in Alzheimer's disease and related disorders. *Nature Reviews Neuroscience* **2007,** 8, 663.

26.   Spillantini, M. G.; Goedert, M. Tau pathology and neurodegeneration. *Lancet Neurol* **2013,** 12, 609-22.

27.   Ballatore, C.; Brunden, K. R.; Huryn, D. M.; Trojanowski, J. Q.; Lee, V. M. Y.; Smith, A. B. Microtubule Stabilizing Agents as Potential Treatment for Alzheimer's Disease and Related Neurodegenerative Tauopathies. *Journal of medicinal chemistry* **2012,** 55, 8979-8996.

28.   Bulic, B.; Pickhardt, M.; Mandelkow, E. Progress and developments in tau aggregation inhibitors for Alzheimer disease. *J Med Chem* **2013,** 56, 4135-55.

29.   Palomo, V.; Martinez, A. Glycogen synthase kinase 3 (GSK-3) inhibitors: a patent update (2014-2015). *Expert Opin Ther Pat* **2017,** 27, 657-666.

30.   Avila, J.; Wandosell, F.; Hernandez, F. Role of glycogen synthase kinase-3 in Alzheimer's disease pathogenesis and glycogen synthase kinase-3 inhibitors. *Expert Rev Neurother* **2010,** 10, 703-10.

31.   Palomo, V.; Perez, D. I.; Roca, C.; Anderson, C.; Rodriguez-Muela, N.; Perez, C.; Morales-Garcia, J. A.; Reyes, J. A.; Campillo, N. E.; Perez-Castillo, A. M.; Rubin, L. L.; Timchenko, L.;

Gil, C.; Martinez, A. Subtly Modulating Glycogen Synthase Kinase 3 beta: Allosteric Inhibitor Development and Their Potential for the Treatment of Chronic Diseases. *J Med Chem* **2017,** 60, 4983-5001.

32.   Bulic, B.; Pickhardt, M.; Schmidt, B.; Mandelkow, E. M.; Waldmann, H.; Mandelkow, E. Development of tau aggregation inhibitors for Alzheimer's disease. *Angew Chem Int Ed Engl* **2009,** 48, 1740-52.

33.   https://clinicaltrials.gov/ct2/show/NCT02380573

34.   Wilcock, G. K.; Gauthier, S.; Frisoni, G. B.; Jia, J.; Hardlund, J. H.; Moebius, H. J.; Bentham, P.; Kook, K. A.; Schelter, B. O.; Wischik, D. J.; Davis, C. S.; Staff, R. T.; Vuksanovic, V.; Ahearn, T.; Bracoud, L.; Shamsi, K.; Marek, K.; Seibyl, J.; Riedel, G.; Storey, J. M. D.; Harrington, C. R.; Wischik, C. M. Potential of Low Dose Leuco-Methylthioninium Bis(Hydromethanesulphonate) (LMTM) Monotherapy for Treatment of Mild Alzheimer's Disease: Cohort Analysis as Modified Primary Outcome in a Phase III Clinical Trial. *J Alzheimers Dis* **2018,** 61, 435-457.

35.   Korcsmáros, T.; Szalay, M. S.; Böde, C.; Kovács, I. A.; Csermely, P. How to design multi-target drugs. *Expert Opinion on Drug Discovery* **2007,** 2, 799-808.

36.   Prati, F.; De Simone, A.; Bisignano, P.; Armirotti, A.; Summa, M.; Pizzirani, D.; Scarpelli, R.; Perez, D. I.; Andrisano, V.; Perez-Castillo, A.; Monti, B.; Massenzio, F.; Polito, L.; Racchi, M.; Favia, A. D.; Bottegoni, G.; Martinez, A.; Bolognesi, M. L.; Cavalli, A. Multitarget drug discovery for Alzheimer's disease: triazinones as BACE-1 and GSK-3beta inhibitors. *Angew Chem Int Ed Engl* **2015,** 54, 1578-82.

37.   de los Ríos, C.; Egea, J.; Marco-Contelles, J.; León, R.; Samadi, A.; Iriepa, I.; Moraleda, I.; Gálvez, E.; García, A. G.; López, M. G.; Villarroya, M.; Romero, A. Synthesis, Inhibitory Activity of Cholinesterases, and Neuroprotective Profile of Novel 1,8-Naphthyridine Derivatives. *Journal of Medicinal Chemistry* **2010,** 53, 5129-5143.

38.   Lorrio, S.; Romero, A.; Gonzalez-Lafuente, L.; Lajarin-Cuesta, R.; Martinez-Sanz, F. J.; Estrada, M.; Samadi, A.; Marco-Contelles, J.; Rodriguez-Franco, M. I.; Villarroya, M.; Lopez, M. G.; de los Rios, C. PP2A ligand ITH12246 protects against memory impairment and focal cerebral ischemia in mice. *ACS Chem Neurosci* **2013,** 4, 1267-77.

39.   Pérez-Areales, F. J.; Di Pietro, O.; Espargaró, A.; Vallverdú-Queralt, A.; Galdeano, C.; Ragusa, I. M.; Viayna, E.; Guillou, C.; Clos, M. V.; Pérez, B.; Sabaté, R.; Lamuela-Raventós, R. M.; Luque, F. J.; Muñoz-Torrero, D. Shogaol–huprine hybrids: Dual antioxidant and anticholinesterase agents with β-amyloid and tau anti-aggregating properties. *Bioorganic & Medicinal Chemistry* **2014,** 22, 5298-5307.

40.   Mariano, M.; Schmitt, C.; Miralinaghi, P.; Catto, M.; Hartmann, R. W.; Carotti, A.; Engel, M. First selective dual inhibitors of tau phosphorylation and Beta-amyloid aggregation, two major pathogenic mechanisms in Alzheimer's disease. *ACS Chem Neurosci* **2014,** 5, 1198-202.

41.   Fuse, S.; Matsumura, K.; Fujita, Y.; Sugimoto, H.; Takahashi, T. Development of dual targeting inhibitors against aggregations of amyloid-β and tau protein. *European Journal of Medicinal Chemistry* **2014,** 85, 228-234.

42.   Okuda, M.; Hijikuro, I.; Fujita, Y.; Teruya, T.; Kawakami, H.; Takahashi, T.; Sugimoto, H. Design and synthesis of curcumin derivatives as tau and amyloid β dual aggregation inhibitors. *Bioorganic & Medicinal Chemistry Letters* **2016,** 26, 5024-5028.

43.   Lajarín-Cuesta, R.; Nanclares, C.; Arranz-Tagarro, J.-A.; González-Lafuente, L.; Arribas, R. L.; Araujo de Brito, M.; Gandía, L.; de los Ríos, C. Gramine Derivatives Targeting Ca2+ Channels and Ser/Thr Phosphatases: A New Dual Strategy for the Treatment of Neurodegenerative Diseases. *Journal of Medicinal Chemistry* **2016,** 59, 6265-6280.

44.   Di Martino, R. M.; De Simone, A.; Andrisano, V.; Bisignano, P.; Bisi, A.; Gobbi, S.; Rampa, A.; Fato, R.; Bergamini, C.; Perez, D. I.; Martinez, A.; Bottegoni, G.; Cavalli, A.; Belluti, F. Versatility of the Curcumin Scaffold: Discovery of Potent and Balanced Dual BACE-1 and GSK-3beta Inhibitors. *J Med Chem* **2016,** 59, 531-44.

45.   Cornec, A. S.; Monti, L.; Kovalevich, J.; Makani, V.; James, M. J.; Vijayendran, K. G.; Oukoloff, K.; Yao, Y.; Lee, V. M.; Trojanowski, J. Q.; Smith, A. B., 3rd; Brunden, K. R.; Ballatore, C. Multitargeted Imidazoles: Potential Therapeutic Leads for Alzheimer's and Other Neurodegenerative Diseases. *J Med Chem* **2017,** 60, 5120-5145.

46.   Panek, D.; Wieckowska, A.; Jonczyk, J.; Godyn, J.; Bajda, M.; Wichur, T.; Pasieka, A.; Knez, D.; Pislar, A.; Korabecny, J.; Soukup, O.; Sepsova, V.; Sabate, R.; Kos, J.; Gobec, S.; Malawska, B. Design, Synthesis, and Biological Evaluation of 1-Benzylamino-2-hydroxyalkyl Derivatives as New Potential Disease-Modifying Multifunctional Anti-Alzheimer's Agents. *ACS Chem Neurosci* **2018**.

47.   Duran-Frigola, M.; Siragusa, L.; Ruppin, E.; Barril, X.; Cruciani, G.; Aloy, P. Detecting similar binding pockets to enable systems polypharmacology. *PLOS Computational Biology* **2017,** 13, e1005522.

48.   Khanfar, M. A.; Hill, R. A.; Kaddoumi, A.; El Sayed, K. A. Discovery of novel GSK-3beta inhibitors with potent in vitro and in vivo activities and excellent brain permeability using combined ligand- and structure-based virtual screening. *J Med Chem* **2010,** 53, 8534-45.

49.   Arfeen, M.; Bhagat, S.; Patel, R.; Prasad, S.; Roy, I.; Chakraborti, A. K.; Bharatam, P. V. Design, synthesis and biological evaluation of 5-benzylidene-2-iminothiazolidin-4-ones as selective GSK-3beta inhibitors. *Eur J Med Chem* **2016,** 121, 727-736.

50.   Martinez, A.; Alonso, M.; Castro, A.; Perez, C.; Moreno, F. J. First non-ATP competitive glycogen synthase kinase 3 beta (GSK-3beta) inhibitors: thiadiazolidinones (TDZD) as potential drugs for the treatment of Alzheimer's disease. *J Med Chem* **2002,** 45, 1292-9.

51.   Bulic, B.; Pickhardt, M.; Khlistunova, I.; Biernat, J.; Mandelkow, E. M.; Mandelkow, E.; Waldmann, H. Rhodanine-based tau aggregation inhibitors in cell models of tauopathy. *Angew Chem Int Ed Engl* **2007,** 46, 9215-9.

52.   Ono, M.; Hayashi, S.; Matsumura, K.; Kimura, H.; Okamoto, Y.; Ihara, M.; Takahashi, R.; Mori, H.; Saji, H. Rhodanine and thiohydantoin derivatives for detecting tau pathology in Alzheimer's brains. *ACS Chem Neurosci* **2011,** 2, 269-75.

53.   Mendgen, T.; Steuer, C.; Klein, C. D. Privileged scaffolds or promiscuous binders: a comparative study on rhodanines and related heterocycles in medicinal chemistry. *J Med Chem* **2012,** 55, 743-53.

54.   Capuzzi, S. J.; Muratov, E. N.; Tropsha, A. Phantom PAINS: Problems with the Utility of Alerts for Pan-Assay INterference CompoundS. *J Chem Inf Model* **2017,** 57, 417-427.

55.   Jasial, S.; Hu, Y.; Bajorath, J. How Frequently Are Pan-Assay Interference Compounds Active? Large-Scale Analysis of Screening Data Reveals Diverse Activity Profiles, Low Global Hit Frequency, and Many Consistently Inactive Compounds. *J Med Chem* **2017,** 60, 3879-3886.

56.   Baell, J. B.; Nissink, J. W. M. Seven Year Itch: Pan-Assay Interference Compounds (PAINS) in 2017-Utility and Limitations. *ACS Chem Biol* **2018,** 13, 36-44.

57.   Pouliot, M.; Jeanmart, S. Pan Assay Interference Compounds (PAINS) and Other Promiscuous Compounds in Antifungal Research. *J Med Chem* **2016,** 59, 497-503.

58.   Baell, J. B. Observations on screening-based research and some concerning trends in the literature. *Future Med Chem* **2010,** 2, 1529-46.

59.   Baell, J. B.; Ferrins, L.; Falk, H.; Nikolakopoulos, G. PAINS: Relevance to Tool Compound Discovery and Fragment-Based Screening. *Australian Journal of Chemistry* **2013,** 66, 1483-1494.

60.https://www.clinicaltrials.gov/ct2/show/NCT01931566?term=pioglitazone%2C+alzheimer&rank=1

61.   Cisek, K.; Cooper, G. L.; Huseby, C. J.; Kuret, J. Structure and mechanism of action of tau aggregation inhibitors. *Current Alzheimer research* **2014,** 11, 918-927.

62.   Reinke, A. A.; Gestwicki, J. E. Insight into amyloid structure using chemical probes. *Chem Biol Drug Des* **2011,** 77, 399-411.

63.	Bhat, B. A.; Ponnala, S.; Sahu, D. P.; Tiwari, P.; Tripathi, B. K.; Srivastava, A. K. Synthesis and antihyperglycemic activity profiles of novel thiazolidinedione derivatives. *Bioorg Med Chem* **2004,** 12, 5857-64.

64.	Zhang, Y.; Zhou, Z. A Solvent-Free Protocol for the Green Synthesis of 5-Arylidene-2,4-thiazolidinediones Using Ethylenediamine Diacetate as Catalyst. *Organic Chemistry International* **2012,** 2012, 5.

65.	Mao, F.; Huang, L.; Luo, Z.; Liu, A.; Lu, C.; Xie, Z.; Li, X. O-Hydroxyl- or o-amino benzylamine-tacrine hybrids: multifunctional biometals chelators, antioxidants, and inhibitors of cholinesterase activity and amyloid-beta aggregation. *Bioorg Med Chem* **2012,** 20, 5884-92.

66.	Qabaja, G.; Jones, G. B. Annulation strategies for benzo[b]fluorene synthesis: efficient routes to the kinafluorenone and WS-5995 antibiotics. *J Org Chem* **2000,** 65, 7187-94.

67.	Baki, A.; Bielik, A.; Molnar, L.; Szendrei, G.; Keseru, G. M. A high throughput luminescent assay for glycogen synthase kinase-3beta inhibitors. *Assay Drug Dev Technol* **2007,** 5, 75-83.

68.	Perez, D. I.; Palomo, V.; Perez, C.; Gil, C.; Dans, P. D.; Luque, F. J.; Conde, S.; Martinez, A. Switching reversibility to irreversibility in glycogen synthase kinase 3 inhibitors: clues for specific design of new compounds. *J Med Chem* **2011,** 54, 4042-56.

69.	Rankovic, Z. CNS Drug Design: Balancing Physicochemical Properties for Optimal Brain Exposure. *Journal of Medicinal Chemistry* **2015,** 58, 2584-2608.

70.	Di, L.; Kerns, E. H.; Fan, K.; McConnell, O. J.; Carter, G. T. High throughput artificial membrane permeability assay for blood-brain barrier. *Eur J Med Chem* **2003,** 38, 223-32.

71.	Crivori, P.; Cruciani, G.; Carrupt, P. A.; Testa, B. Predicting blood-brain barrier permeation from three-dimensional molecular structure. *J Med Chem* **2000,** 43, 2204-16.

72.	Contestabile, A. Cerebellar granule cells as a model to study mechanisms of neuronal apoptosis or survival in vivo and in vitro. *Cerebellum* **2002,** 1, 41-55.

73.	Willson, T. M.; Brown, P. J.; Sternbach, D. D.; Henke, B. R. The PPARs: from orphan receptors to drug discovery. *J Med Chem* **2000,** 43, 527-50.

74. Fitzpatrick, A. W. P.; Falcon, B.; He, S.; Murzin, A. G.; Murshudov, G.; Garringer, H. J.; Crowther, R. A.; Ghetti, B.; Goedert, M.; Scheres, S. H. W. Cryo-EM structures of tau filaments from Alzheimer's disease. *Nature* **2017,** 547, 185-190.

75. Li, W.; Sperry, J. B.; Crowe, A.; Trojanowski, J. Q.; Smith, A. B., 3rd; Lee, V. M. Inhibition of tau fibrillization by oleocanthal via reaction with the amino groups of tau. *J Neurochem* **2009,** 110, 1339-51.

76. Zheng, J.; Liu, C.; Sawaya, M. R.; Vadla, B.; Khan, S.; Woods, R. J.; Eisenberg, D.; Goux, W. J.; Nowick, J. S. Macrocyclic beta-sheet peptides that inhibit the aggregation of a tau-protein-derived hexapeptide. *J Am Chem Soc* **2011,** 133, 3144-57.

77. Mohamed, T.; Hoang, T.; Jelokhani-Niaraki, M.; Rao, P. P. Tau-derived-hexapeptide 306VQIVYK311 aggregation inhibitors: nitrocatechol moiety as a pharmacophore in drug design. *ACS Chem Neurosci* **2013,** 4, 1559-70.

78. Frenkel-Pinter, M.; Tal, S.; Scherzer-Attali, R.; Abu-Hussien, M.; Alyagor, I.; Eisenbaum, T.; Gazit, E.; Segal, D. Naphthoquinone-Tryptophan Hybrid Inhibits Aggregation of the Tau-Derived Peptide PHF6 and Reduces Neurotoxicity. *J Alzheimers Dis* **2016,** 51, 165-78.

79. Lunven, L.; Bonnet, H.; Yahiaoui, S.; Yi, W.; Da Costa, L.; Peuchmaur, M.; Boumendjel, A.; Chierici, S. Disruption of Fibers from the Tau Model AcPHF6 by Naturally Occurring Aurones and Synthetic Analogues. *ACS Chem Neurosci* **2016,** 7, 995-1003.

80. Wang, C. K.; Northfield, S. E.; Huang, Y. H.; Ramos, M. C.; Craik, D. J. Inhibition of tau aggregation using a naturally-occurring cyclic peptide scaffold. *Eur J Med Chem* **2016,** 109, 342-9.

81. Biancalana, M.; Koide, S. Molecular mechanism of Thioflavin-T binding to amyloid fibrils. *Biochim Biophys Acta* **2010,** 1804, 1405-12.

82. Taniguchi, S.; Suzuki, N.; Masuda, M.; Hisanaga, S.; Iwatsubo, T.; Goedert, M.; Hasegawa, M. Inhibition of heparin-induced tau filament formation by phenothiazines, polyphenols, and porphyrins. *J Biol Chem* **2005,** 280, 7614-23.

83.   Wille, H. D., G.; Biernat, J.; Mandelkow, E.M.; Mandelkow, E. . Alzheimer-like paired helical filaments and antiparallel dimers formed from microtubule-associated protein tau in vitro. *The Journal of Cell Biology* **1992,** 118, 573-584.

84.   Paudel, H. K.; Li, W. Heparin-induced conformational change in microtubule-associated protein Tau as detected by chemical cross-linking and phosphopeptide mapping. *J Biol Chem* **1999,** 274, 8029-38.

85.   Wilham, J. M.; Orrú, C. D.; Bessen, R. A.; Atarashi, R.; Sano, K.; Race, B.; Meade-White, K. D.; Taubner, L. M.; Timmes, A.; Caughey, B. Rapid End-Point Quantitation of Prion Seeding Activity with Sensitivity Comparable to Bioassays. *PLOS Pathogens* **2010,** 6, e1001217.

86.   Wang, J.; Tung, Y. C.; Wang, Y.; Li, X. T.; Iqbal, K.; Grundke-Iqbal, I. Hyperphosphorylation and accumulation of neurofilament proteins in Alzheimer disease brain and in okadaic acid-treated SY5Y cells. *FEBS Lett* **2001,** 507, 81-7.

87.   Chen, Z.; Chen, B.; Xu, W. F.; Liu, R. F.; Yang, J.; Yu, C. X. Effects of PTEN inhibition on regulation of tau phosphorylation in an okadaic acid-induced neurodegeneration model. *Int J Dev Neurosci* **2012,** 30, 411-9.

88.   Zhang, Z.; Simpkins, J. W. An okadaic acid-induced model of tauopathy and cognitive deficiency. *Brain Res* **2010,** 1359, 233-46.

89.   Davis, M. I.; Hunt, J. P.; Herrgard, S.; Ciceri, P.; Wodicka, L. M.; Pallares, G.; Hocker, M.; Treiber, D. K.; Zarrinkar, P. P. Comprehensive analysis of kinase inhibitor selectivity. *Nat Biotechnol* **2011,** 29, 1046-51.

90.   Swords, R.; Mahalingam, D.; O'Dwyer, M.; Santocanale, C.; Kelly, K.; Carew, J.; Giles, F. Cdc7 kinase - a new target for drug development. *Eur J Cancer* **2010,** 46, 33-40.

91.   Singh, T. J.; Grundke-Iqbal, I.; Iqbal, K. Phosphorylation of tau protein by casein kinase-1 converts it to an abnormal Alzheimer-like state. *J Neurochem* **1995,** 64, 1420-3.

92. Maccari, R.; Ottana, R.; Curinga, C.; Vigorita, M. G.; Rakowitz, D.; Steindl, T.; Langer, T. Structure-activity relationships and molecular modelling of 5-arylidene-2,4-thiazolidinediones active as aldose reductase inhibitors. *Bioorg Med Chem* **2005,** 13, 2809-23.

93. Aldrich, C.; Bertozzi, C.; Georg, G. I.; Kiessling, L.; Lindsley, C.; Liotta, D.; Merz, K. M., Jr.; Schepartz, A.; Wang, S. The Ecstasy and Agony of Assay Interference Compounds. *J Med Chem* **2017,** 60, 2165-2168.

94. Copeland, R. A. Drug–Target Residence Time. In *Evaluation of Enzyme Inhibitors in Drug Discovery*, 2013; pp 318-325.

95. Avonto, C.; Taglialatela-Scafati, O.; Pollastro, F.; Minassi, A.; Di Marzo, V.; De Petrocellis, L.; Appendino, G. An NMR spectroscopic method to identify and classify thiol-trapping agents: revival of Michael acceptors for drug discovery? *Angew Chem Int Ed Engl* **2011,** 50, 467-71.

96. Torres, J. L.; Lozano, C.; Julià, L.; Sánchez-Baeza, F. J.; Anglada, J. M.; Centelles, J. J.; Cascante, M. Cysteinyl-flavan-3-ol Conjugates from Grape Procyanidins. Antioxidant and Antiproliferative Properties. *Bioorganic & Medicinal Chemistry* **2002,** 10, 2497-2509.

97. Arsovska, E.; Trontelj, J.; Zidar, N.; Tomasic, T.; Masic, L. P.; Kikelj, D.; Plavec, J.; Zega, A. Evaluation of Michael-type acceptor reactivity of 5-benzylidenebarbiturates, 5-benzylidenerhodanines, and related heterocycles using NMR. *Acta Chim Slov* **2014,** 61, 637-44.

98. Polazzi, E.; Mengoni, I.; Caprini, M.; Pena-Altamira, E.; Kurtys, E.; Monti, B. Copper-zinc superoxide dismutase (SOD1) is released by microglial cells and confers neuroprotection against 6-OHDA neurotoxicity. *Neurosignals* **2013,** 21, 112-28.

99. Pena-Altamira, E.; Polazzi, E.; Moretto, E.; Lauriola, M.; Monti, B. The transcription factor CCAAT enhancer-binding protein beta protects rat cerebellar granule neurons from apoptosis through its transcription-activating isoforms. *Eur J Neurosci* **2014,** 39, 176-85.

100. Chaudhary, N.; Singh, S.; Nagaraj, R. Morphology of self-assembled structures formed by short peptides from the amyloidogenic protein tau depends on the solvent in which the peptides are dissolved. *Journal of Peptide Science* **2009,** 15, 675-684.

Table of Contents graphic

GSK-3β

4 - 38

Tau aggregates